Energy transfer between carotenoids and bacteriochlorophylls in light-harvesting complex II of purple bacteria

Ana Damjanović, Thorsten Ritz, and Klaus Schulten
Beckman Institute and Department of Physics, University of Illinois at Urbana—Champaign, Urbana, Illinois 61801
(Received 5 December 1997; revised manuscript received 29 October 1998)

In photosynthetic light-harvesting systems carotenoids and chlorophylls jointly absorb light and transform its energy within about a picosecond into electronic singlet excitations of the chlorophylls only. This paper investigates this process for the light-harvesting complex II of the purple bacterium *Rhodospirillum molischianum*, for which a structure and, hence, the exact arrangement of the participating bacteriochlorophylls and carotenoids have recently become known. Based on this structure and on CI expansions of the electronic states of individual chromophores (bacteriochlorophylls and carotenoids) as well as on an exciton description of a circular aggregate of bacteriochlorophylls, the excitation transfer between carotenoids and bacteriochlorophylls is described by means of Fermi's golden rule. The electronic coupling between the various electronic excitations is determined for all orders of multipoles (Coulomb mechanism) and includes the electron exchange (Dexter mechanism) term. The rates and efficiencies for different pathways of excitation transfer, e.g., $1^1B_u^+$(carotenoid)$\rightarrow$bacteriochlorophyll aggregate and $2^1A_g^-$(carotenoid)$\rightarrow$ bacteriochlorophyll aggregate, are compared. The results show that in LH-II the Coulomb mechanism is dominant for the transfer of singlet excitations. The $1^1B_u^+ \rightarrow Q_x$ pathway appears to be partially efficient, while the $2^1A_g^- \rightarrow Q_y$ pathway, in our description, which does not include vibrational levels, is inefficient. An improved treatment of the excitation transfer from the $2^1A_g^-$ state is required to account for observed transfer rates. Exciton splitting of bacteriochlorophyll Q_y excitations slightly accelerates the excitation transfer from the $2^1A_g^-$ state, while it plays a crucial role in accelerating the transfer from the *B*800 BChl Q_y state. Photoprotection of bacteriochlorophylls through triplet quenching is investigated, too. The results suggest that eight of the 16 *B*850 bacteriochlorophylls in LH-II of *Rhodospirillum molischianum* are protected well by eight carotenoids observed in the x-ray structure of the protein. The remaining eight *B*850 bacteriochlorophylls can transfer their triplet excitation energy efficiently to their neighboring protected bacteriochlorophylls. Eight *B*800 bacteriochlorophylls appear not to be protected well by the observed carotenoids. [S1063-651X(98)11007-3]

PACS number(s): 87.15.Rn, 71.35.−y, 33.50.Hv

I. INTRODUCTION

Carotenoids perform two major roles in photosynthesis as partners of the usually more prevalent chlorophylls: light harvesting and photoprotection. Carotenoids absorb radiation in the visible region inaccessible to chlorophylls and transfer the absorbed energy to chlorophylls which channel it into the photosynthetic reaction center. For example, in the light-harvesting complex II (LH-II) of the purple bacterium *Rhodospirillum (Rs.) molischianum*, eight carotenoids (lycopene) absorb light at 500 nm, whereas 24 bacteriochlorophylls (BChl's) absorb at 800 nm and 850 nm [1,2]. In peridinin-chlorophyll-protein, a light-harvesting protein of dinoflagellates, carotenoids serve actually as the main light absorbers with a carotenoid:chlorophyll ratio of 4:1 [3].

If carotenoidless mutants of the photosynthetic purple bacteria are exposed to light and oxygen, their bacteriochlorophylls (BChl's) are destroyed and the organisms die [4,5]. This photo-oxidative death is thought to be primarily due to excitation of singlet oxygen $^1O_2^*$ through excitation transfer from triplet excited bacteriochlorophyll [6,7], an unavoidable side product of light harvesting. Singlet oxygen is a strong oxidant that combines rapidly with dienes causing the death of an organism [8]. Carotenoids prevent this photo-oxidation.

The availability of the high-resolution x-ray structure of LH-II of the purple bacteria *Rhodopseudomonas (Rps.) acidophila* [9] and *Rs. molischianum* [10] allows one to study excitation transfer between carotenoids and bacteriochlorophylls involved in light harvesting and photoprotection on the basis of a known geometry of the chromophore aggregate. Figure 1(a) displays the structure of the light-harvesting protein LH-II of *Rs. molischianum*. Figure 1(b) presents only the chromophores contained in the structure, namely eight lycopenes and 24 BChl's. LH-II of *Rs. molischianum* forms an octameric aggregate, possessing a C_8 rotation symmetry, with eight monomer units consisting of an α- and a β-apoprotein, one lycopene, and three BChl's. Figure 2 displays the chromophores of one such unit (LYC, *B*800, *B*850*a* and *B*850*b*). Bacteriochlorophylls from neighboring units (the latter marked with a prime and a star) are also shown in Fig. 2, since the lycopene (LYC) exhibits closest edge-edge distances with BChl's: *B*850*a*′ (3.99 Å), *B*850*b* (4.14 Å), *B*800* BChl (3.23 Å).

Absorption of light by carotenoids and singlet excitation transfer between a carotenoid (excitation donor) and a bacteriochlorophyll (excitation acceptor) constitutes the light-harvesting function of carotenoids. Figure 3 compares the energy levels of the carotenoid and bacteriochlorophyll states involved in the transfer. As measured for LH-II of *Rb. sphaeroides* [11], the bacteriochlorophyll Q_x state absorbs at 590 nm and the BChl Q_y state absorbs at 800 nm for the individual *B*800 BChl's and at 850 nm for the *B*850 BChl's.

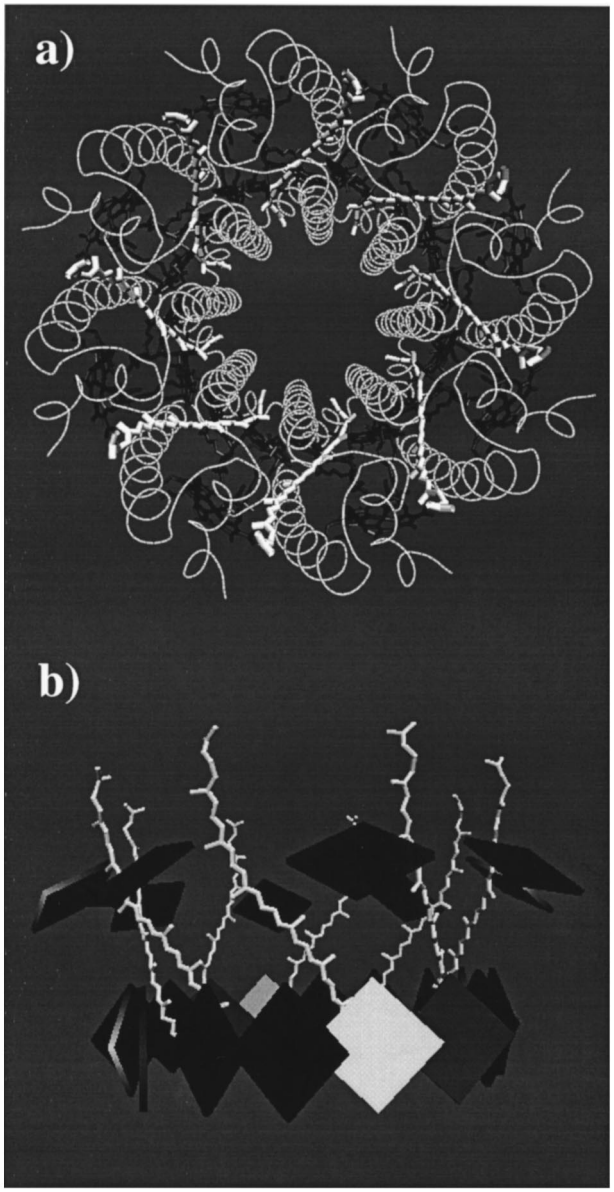

FIG. 1. (a) LH-II of *Rs. molischianum*. This image displays a top view with *N*-termini pointing upward, the apoproteins being represented as C_α-tracing tubes. Eight *B*800 and 16 *B*850 BChl molecules are shown in black. The lycopenes are represented in licorice representation. (b) Arrangement of chromophores in side view. Bacteriochlorophylls are represented as squares; 16 *B*850 BChl's are arranged in the bottom ring and eight *B*800 BChl's in the top ring (produced with the program VMD [70]).

Due to the strong coupling between neighboring *B*850 BChl's, the Q_y excitations form exciton states that, under the assumption of complete exciton delocalization, range in energy from 871 nm to 712 nm [12] as depicted in Fig. 3. Carotenoid's optically allowed $1^1B_u^+$ state [carotenoid states are labeled due to an approximate C_{2h} (A_g,B_u) and due to alternancy (+, -) symmetry] absorbs at 515 nm [13]. The $1^1B_u^+$ state converts rapidly to a longer lived but symmetry forbidden $2^1A_g^-$ excited state [14].

The optically forbidden $2^1A_g^-$ state in polyenes had been characterized both theoretically and spectroscopically [15], e.g., through fluorescence from this state after initial absorption to the $1^1B_u^+$ state. However, for long chains (number of conjugated double bonds exceeding ten) it becomes difficult to detect fluorescence from the $2^1A_g^-$ state due to the widening of the $2^1A_g^-$ to $1^1B_u^+$ energy gap with increasing chain length [14,16–18], which slows down the internal conversion $1^1B_u^+ \rightarrow 2^1A_g^-$, and due to a decrease of the gap to the

FIG. 2. Lycopene (LYC) and its neighboring bacteriochlorophylls. Coordinates are taken from the x-ray structure of LH-II complex of *Rs. molischianum* [10]. Lycopene, *B*850*a*, *B*850*b*, and *B*800 molecules within the outlined area belong to one monomer subunit as defined in [10]. The structure of a monomer subunit is repeated with eight-fold symmetry. It should be noted that the lycopene displays closest contact with BChl's from the neighboring subunits, namely, *B*850*a*′ and *B*800*. The phytol chains as well as some other atoms of the *B*850 BChl's have been omitted for clarity. The figure has been produced with the program VMD [70].

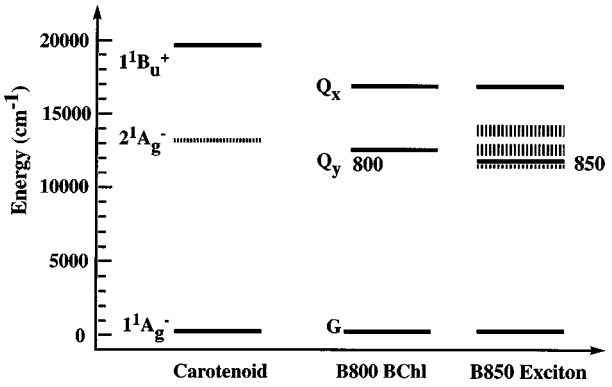

FIG. 3. Excitation energies of carotenoid and BChl states. The carotenoid states are labeled according to their approximate C_{2n} and alternancy symmetry. Next to the carotenoid states, the location of the *B*800 BChl states and of the exciton states of the *B*850 band are shown. Solid lines represent spectroscopically measured energy levels for LH-II of *Rs. molischianum*; dashed lines indicate the estimated excitation energies of the symmetry forbidden $2^1A_g^-$ state in lycopene of *Rs. molischianum* and the symmetry forbidden exciton states of the *B*850 band.

ground state, which increases the rate of internal conversion $2^1A_g^- \rightarrow 1^1A_g^-$. By means of fluorescence spectroscopy the gap between the $2^1A_g^-$ and $1^1A_g^-$ states for carotenoids with $n=3-9$ double bonds has been measured [19] and an extrapolation of the n dependence reflected by the data suggests an excitation energy of the $2^1A_g^-$ state in lycopene ($n=11$) of 757 nm. This is consistent with the recent $2^1A_g^- \rightarrow 1^1A_g^-$ fluorescence measurement for polyenes with 11 conjugated double bonds which places the $2^1A_g^-$ state at 758 nm in n-hexane and at 704 nm in CS_2 [20].

Noting that the carotenoid $1^1B_u^+$ state is absorbing at a similar wavelength as the Q_x BChl state and that the $2^1A_g^-$ state is close in energy to the Q_y state of BChl, two natural pathways of excitation transfer arise: excitation transfer $1^1B_u^+ \rightarrow Q_x$ and excitation transfer $2^1A_g^- \rightarrow Q_y$, the latter preceded by the internal conversion $1^1B_u^+ \rightarrow 2^1A_g^-$. Excitation transfer from lycopene could proceed to both $B800$ and $B850$ BChl's.

The carotenoid $\rightarrow$ BChl transfer time had been determined to be 200 fs for the $B850$ BChl band in *Rb. sphaeroides*, with an overall efficiency of 0.95 [21]. The shortening of the $1^1B_u^+$ state lifetime from 200 fs in CS_2 [22] to 80 fs in the protein environment of LH-II of *Rb. sphaeroides* [23], suggests an energy transfer time of 135 fs with an efficiency of approximately 40%. The lifetime of 9.1 ps of the $2^1A_g^-$ state in cyclohexane [11] is shortened to 2 ps in LH-II [24] indicating that the optically forbidden $2^1A_g^-$ state can also efficiently transfer energy with a transfer time of 2.5 ps.

The $1^1B_u^+ \rightarrow Q_x$ excitation transfer was thought to occur via the Förster mechanism [25], originating from coupling between transition dipole moments of molecular moieties, the coupling representing the dominant term in a multipole-multipole expansion of the respective Coulomb interaction. However, in the case of excitation transfer between chromophores in LH-II, where the distance between chromophores is smaller than the overall size of chromophores themselves, the multipole expansion of Coulomb interaction and particularly the dipole-dipole approximation cease to apply. Even at distances of 20 Å (we note here that the length of the conjugated system in lycopene is approximately 25 Å) the higher-order multipole contributions to the Coulomb interaction between different chromophore states in LH-II can still be on the order of the dipolar contribution [26]. Especially, excitation transfer involving the dipole forbidden $2^1A_g^-$ state is not accounted for at the dipole-dipole level, but requires either vibrational borrowing of oscillator strength or the inclusion of higher-order multipoles, e.g., quadrupole-dipole. One therefore needs to account for the full Coulomb interaction between participating chromophore states (Coulomb mechanism), and determine the respective Coulomb coupling without evoking the multipole expansion, as also suggested in [27].

An alternative to transfer through the Coulomb mechanism is, in principle, transfer through electron exchange, i.e., through the so-called Dexter mechanism [28–30]. In this case, exact knowledge of the geometry of the carotenoid-BChl aggregate is crucial since electron exchange coupling decays rapidly with the edge-edge distance between donor and acceptor. The main goal of recent spectroscopic and theoretical investigations on LH-II is to determine how the mentioned mechanisms contribute to light harvesting and which overall excitation transfer rates result.

Before the solution of the structures of LH-II [9,10], Nagae *et al.* [27] had calculated rates for carotenoid $\rightarrow$ BChl excitation transfer for hypothetical configurations of carotenoid and BChl. The authors argue that the excitation transfer can occur from both the $1^1B_u^+$ and the optically forbidden $2^1A_g^-$ state once the asymmetry of carotenoids is taken into account. The authors compared also the relative efficiencies of the Dexter mechanism and the Coulomb mechanism and determined that the Coulomb mechanism is much more effective than the Dexter mechanism. Recently, a calculation of transfer rates from the $1^1B_u^+$ state through the Coulomb mechanism based on the x-ray crystallographic structure of *Rps. acidophila* has been reported [26]. These calculations demonstrate the breakdown of the dipole approximation for transfer between the optically allowed states of chromophores in LH-II. However, in [26] transfer through the Dexter mechanism and from the optically forbidden $2^1A_g^-$ state have not been studied.

As photoprotecting agents, carotenoids prevent photo-oxidation by quenching singlet oxygen, $^1O_2^*$, into triplet states (scavenging)

$$^1O_2^* + {}^1\mathrm{Car} \rightarrow {}^3\mathrm{Car}^* + {}^3O_2 . \tag{1.1}$$

This requires the energy of the lowest carotenoid triplet state to be lower than the excitation energy of 0.97 eV [31] of $^1O_2^*$. In addition, carotenoids efficiently prevent the production of singlet oxygen [32] by quenching the triplet excited states of BChl according to

$$^3\mathrm{BChl}^* + {}^1\mathrm{Car} \rightarrow {}^1\mathrm{BChl} + {}^3\mathrm{Car}^*, \tag{1.2}$$

before BChl can interact with molecular oxygen. This triplet quenching reaction has been demonstrated in several photosynthetic systems [33,34], which implies that the triplet carotenoid state lies energetically below the triplet state of BChl. The excitation energy of the triplet carotenoid state could not, until now, be measured directly. It is known that the excitation energy decreases with a larger number of conjugated double bonds. Theoretical estimates [35,36] predict that carotenoids with more than seven conjugated double bonds are able to quench the triplet chlorophyll state and that carotenoids with nine or more double bonds can quench the singlet oxygen state. Since *in vivo* experiments indicate clearly that carotenoids with nine or more conjugated double bonds offer efficient protection against photo-oxidation, while carotenoids with less double bonds do not [37–39], it is reasonable to assume that the triplet state of carotenoids with nine or more double bonds lies energetically below the $^1O_2^*$ state.

Since the photoprotection function of carotenoids involves triplet excitation transfer [cf. Eq. (1.2)], the Coulomb mechanism, which conserves the spin state of both donor and acceptor, can be ruled out; the only possible mechanism for the transfer is the Dexter mechanism [28]. For the latter to be efficient it is necessary that the chromophores involved are in close proximity, since exchange coupling involves electron tunneling and, therefore, decreases exponentially with distance. The authors in [27] argue that the Dexter mechanism

is nearly 100% efficient at a distance of approximately 3.5 Å, since the lifetime of the donor BChl triplet state is extremely long, approximately 10 μs [40]. This argument demonstrates that knowledge of the geometry of the carotenoid-BChl aggregate in LH-II, as documented in Figs. 1,2, is a necessary prerequisite to derive any conclusions about the rates of triplet energy transfer in LH-II.

In this paper, we study the excitation transfer pathways in LH-II of *Rs. molischianum* by evaluating the rates of excitation transfer between the lycopene, *B*800 BChl, and *B*850 BChl moieties. We will first summarize the theory underlying excitation transfer due to the Coulomb and the Dexter mechanism. On the basis of the atomic level structure of LH-II of *Rs. molischianum* [10] (as shown in Figs. 1,2), of available spectroscopic data, and of a quantum mechanical description of the electronic structure of lycopene and bacteriochlorophylls we will discuss the pathways for both singlet and triplet excitation transfer.

II. THEORY AND METHODS

A. Electronic coupling for excitation transfer

The rate of transfer of electronic excitation from donor D to acceptor A can be evaluated by means of the well-known expression [25,28]

$$k_{DA}=\frac{2\pi}{\hbar}|U_{DA}|^2 J_{DA}, \quad J_{DA}=\int S_D(E)S_A(E)dE. \tag{2.1}$$

Here U_{DA} describes the electronic coupling between donor and acceptor; J_{DA} represents the spectral overlap integral, where $S_D(E)$ and $S_A(E)$ define the normalized donor emission and acceptor absorption spectrum, respectively. Following the authors in [27] we approximate rather crudely $S_D(E)$ and $S_A(E)$ by Gaussians

$$S_{D(A)}(E)=(2\pi\sigma^2_{D(A)})^{-1/2}\exp[-(E-E_{D(A)})^2/2\sigma^2_{D(A)}], \tag{2.2}$$

where $\sigma_{D(A)}=(\Gamma_{D(A)}/2)(2\ln 2)^{-1/2}$. $E_{D(A)}$ is the energy of the emission or absorption maximum and $\Gamma_{D(A)}$ is the full width at half-maximum. The values of $E_{D(A)}$ and $\Gamma_{D(A)}$ are estimated from the observed emission and absorption spectra.

The electronic coupling U_{DA} arises from the Coulomb interaction in the donor-acceptor pair. This interaction can be expressed as

$$\frac{1}{2}\sum_{\substack{m,n,p,q\\ \in I_D\cup I_A}}\sum_{\sigma,\sigma'}(\phi_m\phi_n|\phi_p\phi_q)c^\dagger_{m\sigma}c^\dagger_{p\sigma'}c_{q\sigma'}c_{n\sigma}, \tag{2.3}$$

where $c^\dagger_{m\sigma}$, $c_{n\sigma'}$ denote the fermion creation and annihilation operators that create and annihilate, respectively, electrons with spins σ and σ' in the mutually orthogonal atomic orbitals ϕ_m and ϕ_n. I_D, I_A denote the set of atomic orbital indices of the donor and acceptor molecules, and we defined

$$(\phi_m\phi_p|\phi_n\phi_q)=\int\int d\vec{r}_1 d\vec{r}_2\phi^*_m(\vec{r}_1)\phi_p(\vec{r}_1)\frac{e^2}{|\vec{r}_1-\vec{r}_2|}\phi^*_n(\vec{r}_2)\phi_q(\vec{r}_2). \tag{2.4}$$

The intramolecular contributions to Eq. (2.3), arising from the sums $\Sigma_{m,n,p,q\in I_D}$ and $\Sigma_{m,n,p,q\in I_A}$, are accounted for in determining the intramolecular (donor, acceptor) electronic excitations; the intermolecular contributions, e.g., $\Sigma_{m,p\in I_D,n,q\in I_A}$ and $\Sigma_{m,q\in I_D,n,p\in I_A}$, are the perturbations that induce the electronic excitation transfer as described by Eq. (2.1). These contributions can be written, exploiting the anticommutation properties of fermion operators,

$$\hat{V}=\sum_{\substack{i,j,\in I_D\\ \sigma}}\sum_{\substack{R,S,\in I_A\\ \sigma'}}[(\phi_i\phi_j|\phi_R\phi_S)c^\dagger_{i\sigma}c_{j\sigma}c^\dagger_{R\sigma'}c_{S\sigma'} -(\phi_i\phi_S|\phi_R\phi_j)c^\dagger_{i\sigma}c_{j\sigma'}c^\dagger_{R\sigma'}c_{S\sigma}]. \tag{2.5}$$

The initial and final electronic states involved in the excitation transfer are assumed to be products of intramolecular donor and acceptor ground and excited states $|\Psi_D\rangle$, $|\Psi^*_D\rangle$, $|\Psi_A\rangle$, $|\Psi^*_A\rangle$, namely, $|\text{init}\rangle=|\Psi^*_D\rangle\otimes|\Psi_A\rangle$ and $|\text{fin}\rangle=|\Psi_D\rangle\otimes|\Psi^*_A\rangle$. The electronic coupling U_{DA} in Eq. (2.1) can then be expressed by the matrix element

$$U_{DA}=\langle\text{init}|\hat{V}|\text{fin}\rangle, \tag{2.6}$$

which can be evaluated using Eq. (2.5). The result can be split into two contributions

$$U_{DA}=U^c_{DA}+U^{ex}_{DA}, \tag{2.7}$$

where

$$U^c_{DA}=\sum_{\substack{i,j\\ \in I_D}}\sum_{\substack{R,S\\ \in I_A}}(\phi_i\phi_j|\phi_R\phi_S)\langle\Psi^*_D|\sum_\sigma c^\dagger_{i\sigma}c_{j\sigma}|\Psi_D\rangle \times\langle\Psi_A|\sum_{\sigma'}c^\dagger_{R\sigma'}c_{S\sigma'}|\Psi^*_A\rangle \tag{2.8}$$

describes the direct Coulomb interaction and where

$$U^{ex}_{DA}=-\sum_{\substack{i,j\\ \in I_D}}\sum_{\substack{R,S\\ \in I_A}}\sum_{\sigma,\sigma'}(\phi_i\phi_S|\phi_R\phi_j)\langle\Psi^*_D|c^\dagger_{i\sigma}c_{j\sigma'}|\Psi_D\rangle \times\langle\Psi_A|c^\dagger_{R\sigma'}c_{S\sigma}|\Psi^*_A\rangle \tag{2.9}$$

describes the exchange interaction which is well known in multielectron systems. The term U^c_{DA} in Eq. (2.8) encapsulates the Coulomb mechanism introduced above; in the limit that donor and acceptor are sufficiently separated such that only the leading (in the case of optically allowed excitations $|\Psi_D\rangle\rightarrow|\Psi^*_D\rangle$, $|\Psi_A\rangle\rightarrow|\Psi^*_A\rangle$) dipole-dipole contributions need to be evoked, the coupling is that described originally by Förster [25]. The term U^{ex}_{DA} in Eq. (2.9) encapsulates the Dexter mechanism [28] also introduced above. Due to the close proximity of donor and acceptor (see Fig. 2) and the

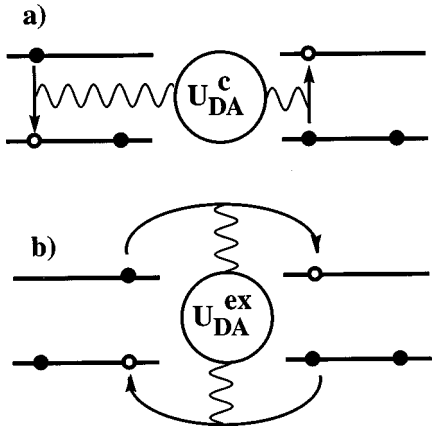

FIG. 4. Schematic representation of (a) the Coulomb and (b) the exchange mechanism of excitation transfer.

involvement of the optically forbidden $2^1A_g^-$ excitation in energy transfer between lycopene and BChl's in LH-II (see Fig. 3), both Eq. (2.8), without evoking the dipolar approximation, and Eq. (2.9) need to be taken into account.

The Coulomb and exchange mechanisms are illustrated in Fig. 4. In case of the Coulomb mechanism, multipole-multipole Coulomb interaction deexcites an initially excited electron on the donor molecule *D* and simultaneously excites an electron on the acceptor molecule *A*. In the case of the Dexter mechanism, excitation is transferred between a donor *D* and an acceptor *A* when an excited electron, initially belonging to *D*, is exchanged for a nonexcited electron initially belonging to *A*. Figure 5 depicts schematically a possible

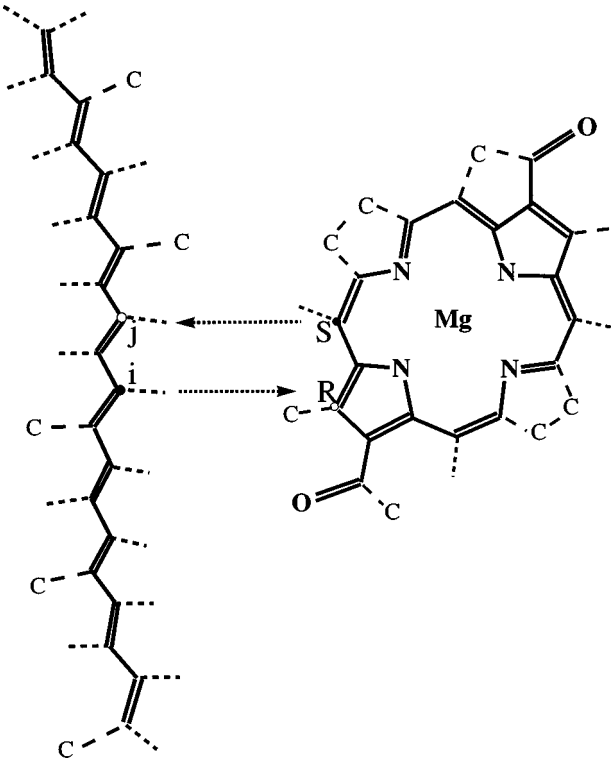

FIG. 5. Schematic representation of conjugated double bonds in LYC_{down} as defined in Sec. II C and the bacteriochlorophyll analog actually employed in the calculations. Representative interacting atoms *i*, *j*, *R*, and *S* are indicated in the figure.

arrangement of atomic orbitals (i,j,R,S) involved in an excitation transfer. We adopt the convention that lower case letters, e.g., (i,j), denote orbitals of the donor while upper case letters, e.g., (R,S), denote orbitals of the acceptor.

B. Spin tensor properties of electronic couplings

The operator $\Sigma_{\sigma,\sigma'} c_{i\sigma}^{\dagger} c_{j\sigma'} c_{R\sigma'}^{\dagger} c_{S\sigma}$, arising in Eq. (2.9), is a rank zero tensor operator for the overall (donor and acceptor) spin, but the intramolecular operators $c_{i\sigma}^{\dagger} c_{j\sigma'}$ and $c_{R\sigma'}^{\dagger} c_{S\sigma}$ can actually be expressed as sums of rank zero and rank one spin operators. Defining

$$\hat{Q} = \frac{1}{2} \sum_{\sigma,\sigma'} c_{i\sigma}^{\dagger} c_{j\sigma'} c_{R\sigma'}^{\dagger} c_{S\sigma}, \tag{2.10}$$

where the prefactor is introduced for convenience, one can expand

$$\hat{Q} = {}^{00}\hat{O}_j^i {}^{00}\hat{O}_S^R - {}^{10}\hat{O}_j^i {}^{10}\hat{O}_S^R + {}^{11}\hat{O}_j^i {}^{1-1}\hat{O}_S^R + {}^{1-1}\hat{O}_j^i {}^{11}\hat{O}_S^R. \tag{2.11}$$

The operators introduced here, ${}^{lm}\hat{O}_j^i$ and ${}^{lm}\hat{O}_S^R$, are of rank *l*, and are defined as

$${}^{00}\hat{O}_j^i = \sqrt{\tfrac{1}{2}} (c_{i\alpha}^{\dagger} c_{j\alpha} + c_{i\beta}^{\dagger} c_{j\beta}), \tag{2.12}$$

$${}^{10}\hat{O}_j^i = \sqrt{\tfrac{1}{2}} (c_{i\alpha}^{\dagger} c_{j\alpha} - c_{i\beta}^{\dagger} c_{j\beta}), \tag{2.13}$$

$${}^{11}\hat{O}_j^i = -c_{i\alpha}^{\dagger} c_{j\beta}, \tag{2.14}$$

$${}^{1-1}\hat{O}_j^i = c_{i\beta}^{\dagger} c_{j\alpha}. \tag{2.15}$$

α and β denote ''up'' and ''down'' spin-$\frac{1}{2}$ states. The tensor operators ${}^{00}\hat{O}_j^i$ do not alter the spin state in the intramolecular transitions $|\Psi_D\rangle \rightarrow |\Psi_D^*\rangle$, $|\Psi_A\rangle \rightarrow |\Psi_A^*\rangle$; the tensor operators ${}^{1m}\hat{O}_j^i$ couple singlet to $(1,m)$ triplet excitations. In case of singlet excitations the matrix elements in Eq. (2.9) are

$$U_{DA}^{ex} = -2 \sum_{\substack{i,j \\ \in I_D}} \sum_{\substack{R,S \\ \in I_A}} (\phi_i \phi_S | \phi_R \phi_j) \langle \Psi_D^* | {}^{00}\hat{O}_j^i | \Psi_D \rangle \times \langle \Psi_A | {}^{00}\hat{O}_S^R | \Psi_A^* \rangle. \tag{2.16}$$

In case that $|\Psi_D^*\rangle$ and $|\Psi_A^*\rangle$ represent $(1,+1)$ triplet excitations, the matrix elements are

$$U_{DA}^{ex} = 2 \sum_{\substack{i,j \\ \in I_D}} \sum_{\substack{R,S \\ \in I_A}} (\phi_i \phi_S | \phi_R \phi_j) \langle \Psi_D^* | {}^{1,1}\hat{O}_j^i | \Psi_D \rangle \times \langle \Psi_A | {}^{1,-1}\hat{O}_S^R | \Psi_A^* \rangle. \tag{2.17}$$

The coupling for triplet excitations $(1,0)$ and $(1,-1)$ yields the same numerical result as the expression above, such that only one type of triplet state needs to be considered.

We note finally that in the present notation the coupling U_{DA}^{c} can be expressed as

$$U_{DA}^{c}=2\sum_{\substack{i,j\\ \in I_D}}\sum_{\substack{R,S\\ \in I_A}}(\phi_i\phi_j|\phi_R\phi_S)\langle\Psi_D^*|^{00}\hat{O}_j^i|\Psi_D\rangle \times\langle\Psi_A|^{00}\hat{O}_S^R|\Psi_A^*\rangle. \quad (2.18)$$

Evaluation of U_{DA} in Eq. (2.1) then requires knowledge of the transition density matrix elements

$$^{l}M_D(i,j)=\langle\Psi_D^*|^{lm}\hat{O}_j^i|\Psi_D\rangle \quad (2.19)$$

and

$$^{l}M_A(R,S)=\langle\Psi_A|^{lm}\hat{O}_S^R|\Psi_A^*\rangle. \quad (2.20)$$

We drop the m dependence on the left-hand side since one expects identical coupling for any of the three triplet states such that the m dependence is immaterial.

C. Carotenoid and bacteriochlorophyll electronic states

The calculation of the transition density matrix elements (2.19,2.20) requires the description of the carotenoid and BChl electronic states involved in the excitation transfer processes. Excitation transfer between BChl's and carotenoids involves exclusively π-π^* transitions.

Figure 5 depicts the conjugated π-electron system of lycopene. Lycopene has 11 conjugated double bonds; however, only 10 double bonds and 20 C atoms are shown in Fig. 5 and employed in our calculations. The latter choice is necessitated by the extreme computational effort to describe the π,π^* states of lycopene. The approximation is not expected to introduce qualitative errors in the predicted lycopene $\rightarrow$ BChl excitation transfer rates since a small difference in the length of the conjugated system leaves the symmetry properties of the transition density matrix elements unchanged and introduces only small quantitative changes. We calculate transition density matrix elements employing two lycopene analogue structures, LYC_{down} and LYC_{up}. LYC_{down} consists of the 20 lycopene C atoms (belonging to the conjugated system) that are closest to *B*850 BChl's and LYC_{up} of the twenty lycopene atoms closer to *B*800 BChl's. All coordinates are taken from the x-ray structure of LH-II of *Rs. molischianum*.

The calculations of the BChl transition density matrix elements are based on the geometry of a symmetric BChl analogue (Fig. 5) rather than on the x-ray structure. This approximation allows one to identify the Q_y and Q_x states. (Identification of the Q_x state of the asymmetric BChl as taken from the x-ray structure is precluded since in this case these states mix strongly with higher-energy excitations.)

In describing the electronic states of BChl the effect of the central magnesium atom has been taken into account by adding two electrons to the conjugated system of the tetrapyrrol ring.

For the required electronic states we choose a semiempirical description as provided by the Pariser-Parr-Pople (PPP) Hamiltonian [41]

TABLE I. Semiempirical parameters of the PPP Hamiltonian as defined in expressions (2.21), (2.22) and (2.23).

$\gamma_0=-2.43$ eV
$Z_k=1.0$
$r_{k,\pm1}=1.35$ Å (double bonds)
$=1.46$ Å (singe bonds)

Carbon (C)	Oxygen (O)	Nitrogen (N)
$I_k=11.16$ eV	$I_k=17.70$ eV	$I_k=14.12$ eV
$R_{kk}=11.13$ eV	$R_{kk}=15.23$ eV	$R_{kk}=12.34$ eV

$$H=\sum_{i<j}Z_iZ_jR_{ij}+\sum_{i,\sigma}\left(-I_i-\sum_{j\neq i}Z_jR_{ij}\right)n_{i\sigma} +\sum_{i\neq j,\sigma}t_{ij}c_{i\sigma}^{+}c_{j\sigma}+\frac{1}{2}\sum_{i,j,\sigma,\tilde{\sigma}}R_{ij}n_{i\sigma}n_{i\tilde{\sigma}}, \quad (2.21)$$

which involves only a minimum number of orbitals, namely, those of π type. $c_{i\sigma}^{+}$ and $c_{j\sigma}$ act on the mutually orthogonal atomic π orbitals; the operator $n_{i\sigma}=c_{i\sigma}^{+}c_{i\sigma}$ is the corresponding number operator; R_{ij} is the effective electron-electron repulsion integral between an electron in an atomic orbital at site i and one in an orbital at site j; t_{ij} is the core integral between atoms i and j; I_i is the effective ionization potential of an orbital at site i; Z_i is the net charge of the core at atom i that was chosen as $Z_j=1$.

The first term in Eq. (2.21) is constant for fixed geometries and represents the nuclear repulsion. The second term in Eq. (2.21) denotes the energy of an electron placed in the atomic orbital at site i, I_i is the ionization potential at atomic site i, and $-Z_jR_{ij}$ accounts for the attractive Coulomb interaction with another atomic site j. The third term in Eq. (2.21) describes the coupling between different atomic orbitals; it is nonvanishing for nearest-neighboring orbitals only, and is evaluated according to the empirical formula [41]

$$t_{ij}=\gamma_0+3.21(r_{ij}-1.397\ \text{Å}). \quad (2.22)$$

γ_0 is a constant and r_{ij} is the distance between the nuclear sites i and j. The fourth term in (2.21) accounts for the Coulomb interaction between the π electrons and, following [14,17], is expressed by the Ohno formula

$$R_{ij}=14.397\ \text{eV}\left[\left(\frac{2\times14.397\ \text{eV}}{R_{ii}+R_{jj}}\right)^2+\frac{r_{ij}^2}{\text{Å}^2}\right]^{-1/2}. \quad (2.23)$$

The semiempirical parameters for the PPP Hamiltonian are listed in Table I.

A self-consistent field configuration interaction (SCF-CI) calculation was performed including single excited π-electron configurations for the triplet carotenoid states as well as for all bacteriochlorophyll states. Since the singlet carotenoid $2^1A_g^-$ state is dominated by double excited configurations [42], a basis set including both single and double excited configurations was employed for the carotenoid singlet states. The large size of this basis for a polyene with

eleven double bonds, namely, 7503, suggested the use of a 10-bond analogue of lycopene in the calculations below.

π-electron states of polyenes obey a C_{2h} symmetry that involves 180^0 rotation about the symmetry axis (symmetry labels A,B) and the inversion at the symmetry center (symmetry labels g, u). The overall symmetry of the N electron states (here N is the number of C atoms of the conjugated system) is either A_g or B_u [15]. Besides the spatial symmetry, the PPP Hamiltonian of pure polyenes exhibits the so-called alternancy symmetry (see also Appendix), according to which the π-electron states are characterized as ''+'' and ''−'' [41,17]. Accordingly, the carotenoid states involved in our calculation are labeled $1^1A_g^-$ for the ground state, $2^1A_g^-$ for the optically forbidden singlet state, $1^1B_u^+$ for the optically allowed singlet state and $1^3B_u^+$ for the lowest energy triplet state. Singlet ''+'' states are reasonably well described in terms of singly excited π-electron configurations only, while singlet ''−'' states require single and double excited configurations for their description [42]. An inclusion of higher excitations, e.g., triple and quadruple excitations, is required to determine quantitatively the energy gaps between the electronic states of polyenes [16,17], but are not needed to capture the essential character of the low-energy polyene electronic excitations as it relates to excitation transfer rates. Below we will employ the electronic wave functions obtained solely for the purpose of evaluating the transition density matrices (2.19,2.20).

D. Transformation to nonorthogonal orbitals

Coulomb and exchange couplings, U_{DA}^c [Eq. (2.18)] and U_{DA}^{ex} [Eqs. (2.16,2.17)], are expressed in terms of orthogonal atomic orbitals. Standard procedures of calculating Coulomb and exchange integrals, $(\phi_i\phi_j|\phi_R\phi_S)$ and $(\phi_i\phi_S|\phi_R\phi_j)$, however, involve nonorthogonal (e.g., Slater) atomic orbitals $|\tilde{\phi}_i\rangle$, related to the orthogonal orbitals $|\phi_{i'}\rangle$ as

$$|\tilde{\phi}_i\rangle=\sum_{i'} S_{i,i'}^{1/2}|\phi_{i'}\rangle, \tag{2.24}$$

or inversely

$$|\phi_{i'}\rangle=\sum_{i} S_{i,i'}^{-(1/2)}|\tilde{\phi}_i\rangle. \tag{2.25}$$

Here $S_{i,i'}^{1/2}$ ($S_{i,i'}^{-(1/2)}$) are elements of the square root (square root to the minus one) of the positive definite nonorthogonal atomic orbital overlap matrix $S_{i,i'}=S_{i',i}=\langle\tilde{\phi}_{i'}|\tilde{\phi}_i\rangle$. As suggested in [43] we take $S_{i,i'}$ to be 1 when $i=i'$, 0.27 when atoms i and i' are joined by a chemical bond, and zero otherwise.

Employing Eq. (2.25) expression (2.18) can be rewritten in terms of nonorthogonal orbitals (here we use dummy indices i', j', R', and S' to number orthogonal atomic orbitals, and i, j, R, and S for nonorthogonal orbitals)

$$\begin{aligned}U_{DA}^c&=2\sum_{\substack{i',j'\\ \in I_D}}\sum_{\substack{R',S'\\ \in I_A}}(\phi_{i'}\phi_{j'}|\phi_{R'}\phi_{S'})^0M_D(i',j')^0M_A(R',S')\\&=2\sum_{\substack{i,j,i',j'\\ \in I_D}}\sum_{\substack{R,S,R',S'\\ \in I_A}}(\tilde{\phi}_i\tilde{\phi}_j|\tilde{\phi}_R\tilde{\phi}_S)S_{i,i'}^{-(1/2)}S_{j,j'}^{-(1/2)}\\&\quad\times S_{R,R'}^{-(1/2)}S_{S,S'}^{-(1/2)0}M_D(i',j')^0M_A(R',S')\\&=2\sum_{\substack{i,j\\ \in I_D}}\sum_{\substack{R,S\\ \in I_A}}(\tilde{\phi}_i\tilde{\phi}_j|\tilde{\phi}_R\tilde{\phi}_S)^0\tilde{M}_D(i,j)^0\tilde{M}_A(R,S),\end{aligned} \tag{2.26}$$

where

$${}^0\tilde{M}_D(i,j)=\sum_{\substack{i',j'\\ \in I_D}} S_{i,i'}^{-(1/2)}S_{j,j'}^{-(1/2)0}M_D(i',j'), \tag{2.27}$$

$${}^0\tilde{M}_A(R,S)=\sum_{\substack{R',S'\\ \in I_A}} S_{R,R'}^{-(1/2)}S_{S,S'}^{-(1/2)0}M_A(R',S'). \tag{2.28}$$

Similarly, expressions (2.16, 2.17) become

$$\begin{aligned}U_{DA}^{ex}&=(-1)^{l+1}2\sum_{\substack{i',j'\\ \in I_D}}\sum_{\substack{R',S'\\ \in I_A}}(\phi_{i'}\phi_{S'}|\phi_{R'}\phi_{j'})\\&\quad\times{}^lM_D(i',j')\,{}^lM_A(R',S')\\&=(-1)^{l+1}2\sum_{\substack{i,j\\ \in I_D}}\sum_{\substack{R,S\\ \in I_A}}(\tilde{\phi}_i\tilde{\phi}_S|\tilde{\phi}_R\tilde{\phi}_j)\\&\quad\times{}^l\tilde{M}_D(i,j)\,{}^l\tilde{M}_A(R,S),\end{aligned} \tag{2.29}$$

where $l=0$ for singlet excitations and $l=1$ for triplet excitations. Expressions (2.26) and (2.29) show that the couplings can be expressed equivalently in terms of orthogonal and nonorthogonal atomic orbitals. Since we calculate the Coulomb and exchange integrals $(\tilde{\phi}_i\tilde{\phi}_j|\tilde{\phi}_R\tilde{\phi}_S)$ and $(\tilde{\phi}_i\tilde{\phi}_S|\tilde{\phi}_R\tilde{\phi}_j)$ in terms of nonorthogonal orbitals, the transition density matrix elements need to be calculated for nonorthogonal orbitals as well. These matrix elements have been evaluated according to expression (2.27,2.28) and are, for different states and pigments, shown in Figs. 6, 7, and 8.

E. Evaluation of two-electron interactions

The matrix elements $(\tilde{\phi}_i\tilde{\phi}_j|\tilde{\phi}_R\tilde{\phi}_S)$, arising in the Coulomb term (2.26), can be expressed quite accurately in the Mulliken approximation

$$\begin{aligned}(\tilde{\phi}_i\tilde{\phi}_j|\tilde{\phi}_R\tilde{\phi}_S)=\frac{S_{ij}S_{RS}}{4}[&(\tilde{\phi}_i\tilde{\phi}_i|\tilde{\phi}_R\tilde{\phi}_R)+(\tilde{\phi}_i\tilde{\phi}_i|\tilde{\phi}_S\tilde{\phi}_S)\\&+(\tilde{\phi}_j\tilde{\phi}_j|\tilde{\phi}_R\tilde{\phi}_R)+(\tilde{\phi}_j\tilde{\phi}_j|\tilde{\phi}_S\tilde{\phi}_S)].\end{aligned} \tag{2.30}$$

Here S_{ij} (S_{RS}) are the elements of the atomic orbital overlap matrix as defined in the previous section. One can approximate further $(\tilde{\phi}_i\tilde{\phi}_i|\tilde{\phi}_R\tilde{\phi}_R)=e^2/R_{iR}$, etc., where R_{iR} is the

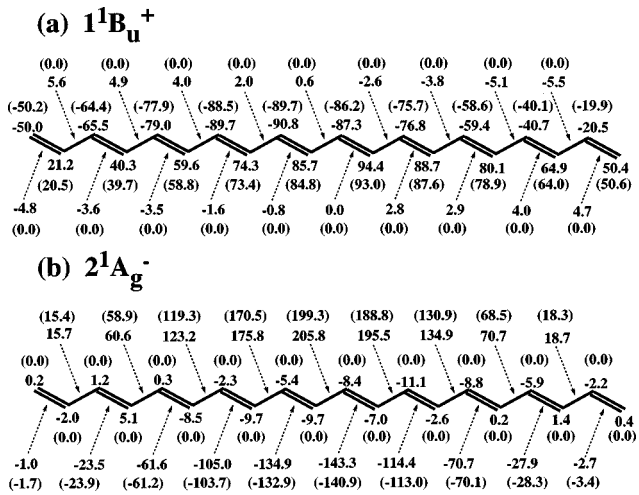

FIG. 6. Transition density matrix elements ${}^0\tilde{M}_D(i,i)$ and ${}^0\tilde{M}_D(i,j)+{}^0\tilde{M}_D(j,i)(i\neq j)$ in units of 10^{-3}, as defined in Eqs. (2.27,2.19) for (a) the $2^1A_g^-\rightarrow 1^1A_g^-$ transition and (b) the $1^1B_u^+\rightarrow 1^1A_g^-$ transition of lycopene (LYC_{down}). Transition density matrix elements expressed in orthogonal atomic orbitals defined in Eq. (2.19), i.e., ${}^0M_D(i,i)$ and ${}^0M_D(i,j)+{}^0M_D(j,i)(i\neq j)$ are shown in brackets. Numbers on atoms correspond to ${}^0\tilde{M}_D(i,i)$, while those on bonds correspond to ${}^0\tilde{M}_D(i,j)+{}^0\tilde{M}_D(j,i)(i\neq j)$.

distance between atomic centers i and R and use also $R_{iR}^{-1}+R_{iS}^{-1}+R_{jR}^{-1}+R_{jS}^{-1}\approx 4R_{ij,RS}^{-1}$, where $R_{ij,RS}$ is the distance between the midpoint of atoms i and j and the midpoint of atoms R and S. Accordingly, we adopt in our calculations the approximation, suggested also in [27],

$$(\tilde{\phi}_i\tilde{\phi}_j|\tilde{\phi}_R\tilde{\phi}_S)=S_{ij}\frac{e^2}{R_{ij,RS}}S_{RS}. \tag{2.31}$$

The exchange coupling decays exponentially with distance and, therefore, the strength of the coupling depends sensitively on the separation between donor and acceptor atoms. One must note in this respect that bridge atoms not belonging to the conjugated π-electron system, but bonded to it, can mediate electron exchange. Figure 9 shows that several atoms at the edges of lycopene and BChl can function as bridge atoms. We include, therefore, in addition to direct electron exchange couplings between the π systems of the chromophores also the electron exchange coupling mediated through bridge atoms.

A bridge consisting of two atoms B (either hydrogen or carbon), located between the $C(2\pi)$ orbitals i and R, is denoted as $C_i(2\pi)-B_{i(H,C)}\cdots B_{R(H,C)}-C_R(2\pi)$ where i(H,C) and R(H,C) are indices for hydrogen or carbon atoms bonded to atoms i and R. The effective coupling through such a bridge can be expressed as [44,45]

$$\beta^{eff}=\frac{\beta}{\Delta E}(\tilde{\phi}_{i(H,C)}\tilde{\phi}_{R(H,C)}|\tilde{\phi}_{R(H,C)}\tilde{\phi}_{i(H,C)})\frac{\beta}{\Delta E}, \tag{2.32}$$

where β is the through-bond exchange interaction between the $C(2\pi)$ π orbital and the bridge orbital, typically about 0.1 eV, and where ΔE is the difference between the energy of the $C(2\pi)$ and the bridge orbitals which is assumed to be 8 eV; $(\tilde{\phi}_{i(H,C)}\tilde{\phi}_{R(H,C)}|\tilde{\phi}_{R(H,C)}\tilde{\phi}_{i(H,C)})$ denotes the electron exchange coupling between the two bridge atomic orbitals. In case of a bridge consisting of a single atom, e.g., for $C_i(2\pi)-B_{i(H,C)}\cdots C_R(2\pi)$, Eq. (2.32) can be expressed as [44,45]

$$\beta^{eff}=\frac{\beta}{\Delta E}(\tilde{\phi}_{i(H,C)}\tilde{\phi}_R|\tilde{\phi}_R\tilde{\phi}_{i(H,C)}), \tag{2.33}$$

where $(\tilde{\phi}_{i(H,C)}\tilde{\phi}_R|\tilde{\phi}_R\tilde{\phi}_{i(H,C)})$ is the electron exchange coupling between the bridge atomic orbital and the $C(2\pi)$ orbital.

Included in our evaluation of bridge-mediated electron exchange are all bridge atoms that are directly bonded to the π systems. The positions of carbon atoms were obtained from the x-ray structure, while the positions of hydrogen atoms were modeled using the program QUANTA [46]. In order to account for both direct and bridge-mediated contributions to the exchange coupling, the exchange integrals $(\tilde{\phi}_i\tilde{\phi}_S|\tilde{\phi}_R\tilde{\phi}_j)$ in Eq. (2.9) were replaced by

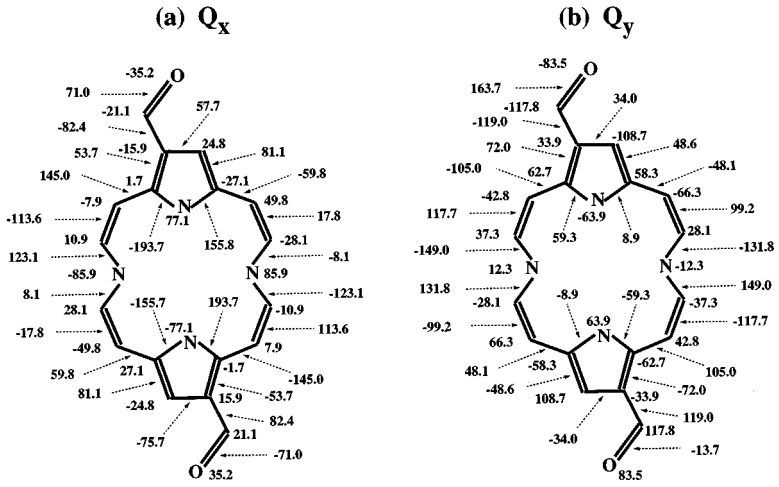

FIG. 7. Transition density matrix elements ${}^0\tilde{M}_A(R,R)$ and ${}^0\tilde{M}_A(R,S)+{}^0\tilde{M}_A(S,R)(R\neq S)$ in units of 10^{-3}, as defined in Eqs. (2.27,2.20) for (a) the $Q_x\rightarrow$ ground state transition and (b) the $Q_y\rightarrow$ ground state transition of bacteriochlorophyll analogue. Numbers on atoms correspond to ${}^0\tilde{M}_A(R,R)$, while those on bonds correspond to ${}^0\tilde{M}_A(R,S)+{}^0\tilde{M}_A(S,R)(R\neq S)$.

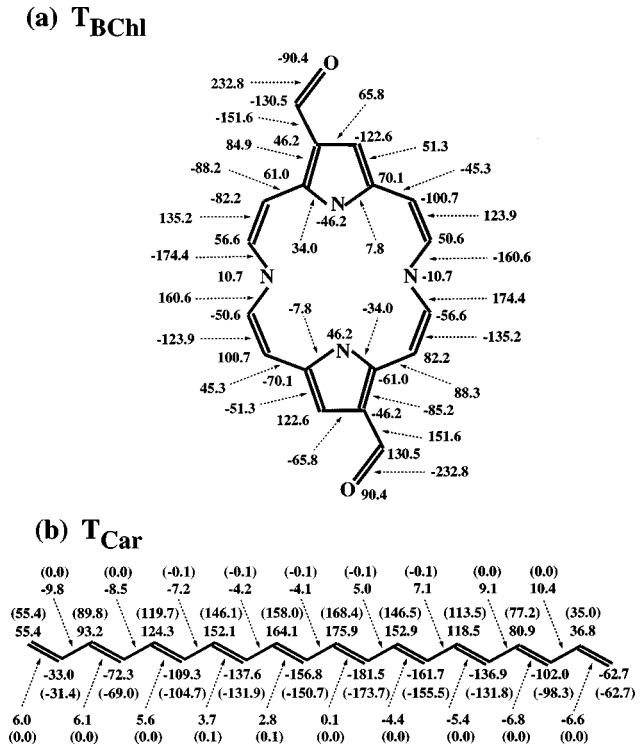

FIG. 8. Transition density matrix elements (a) ${}^1\tilde{M}_D(i,j)$, ${}^0\tilde{M}_D(i,j)+{}^0\tilde{M}_D(j,i)(i\neq j)$ in units of 10^{-3}, for the triplet $\rightarrow$ ground state transition of bacteriochlorophyll analogue and (b) ${}^1\tilde{M}_A(R,S)$, ${}^0\tilde{M}_A(R,S)+{}^0\tilde{M}_A(S,R)(R\neq S)$ in units of 10^{-3}, for the triplet $\rightarrow$ ground state transition of lycopene (LYC_{down}). The matrix elements have been determined according to Eqs. (2.27, 2.19, 2.20).

$$
\begin{aligned}
&(\tilde{\phi}_i\tilde{\phi}_S|\tilde{\phi}_R\tilde{\phi}_j)_{\mathrm{TOTAL}}\\
&\quad=(\tilde{\phi}_i\tilde{\phi}_S|\tilde{\phi}_R\tilde{\phi}_j)+(\tilde{\phi}_{i(H,C)}\tilde{\phi}_S|\tilde{\phi}_R\tilde{\phi}_{i(H,C)})\frac{\beta}{\Delta E}\delta_{i,j}\\
&\qquad+(\tilde{\phi}_i\tilde{\phi}_{R(H,C)}|\tilde{\phi}_{R(H,C)}\tilde{\phi}_j)\frac{\beta}{\Delta E}\delta_{R,S}\\
&\qquad+(\tilde{\phi}_{i(H,C)}\tilde{\phi}_{R(H,C)}|\tilde{\phi}_{R(H,C)}\tilde{\phi}_{i(H,C)})\left(\frac{\beta}{\Delta E}\right)^2\delta_{i,j}\delta_{R,S}.
\end{aligned}
\tag{2.34}
$$

The quantities $(\tilde{\phi}_i\tilde{\phi}_S|\tilde{\phi}_R\tilde{\phi}_j)$, $(\tilde{\phi}_{i(H,C)}\tilde{\phi}_S|\tilde{\phi}_R\tilde{\phi}_{i(H,C)})$, etc., arising in expression (2.34), account for electron exchange involving the atomic orbitals i, j, R, and S for the first exchange integral in Eq. (2.34), or i(H,C), R and S for the second exchange integral, etc. These exchange integrals depend sensitively on the shapes of atomic wave functions. Instead of exploiting single Slater orbitals which decay too quickly with distance for a description of the carbon atomic $2p\pi$ wave functions, we employ SCF $2p\pi$ orbitals that have longer ''tails'' and are more accurate [27],

$$
\tilde{\phi}(\mathrm{SCF}\,2p\pi)=\vec{r}\cdot\hat{z}\sum_{i=1}^{5}a_i(\alpha_i^5/\pi)^{1/2}e^{-\alpha_i r}. \tag{2.35}
$$

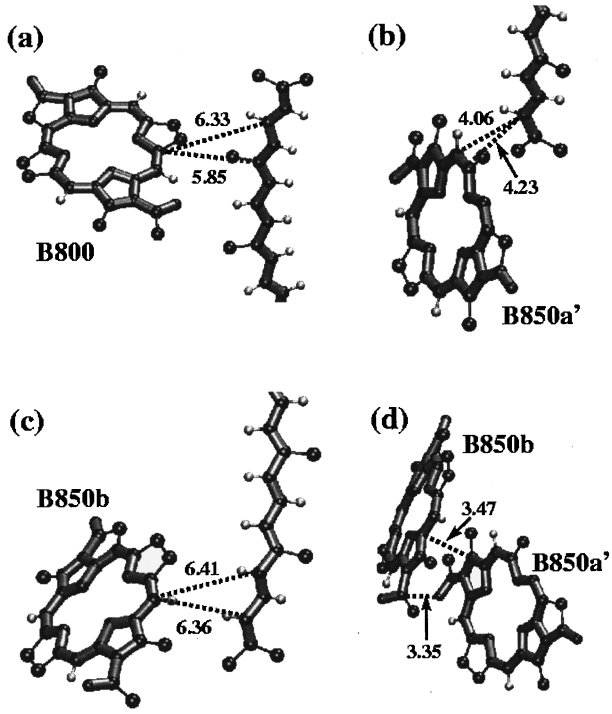

FIG. 9. Geometry of closest contacts between chromophores in LH-II of *Rs. molischianum*. Included are atoms belonging to the conjugated system (connected by thick bonds) and atoms in direct contact with the conjugated system (connected to the latter by thin bonds). All nonhydrogen coordinates are taken from the x-ray structure of *Rs. molischianum* [10], while the hydrogens were modeled with QUANTA [46]. Carbon atoms are in black, hydrogen atoms in light gray. Distances between the conjugated systems are indicated in Å. The distances between *B*850*a'* BChl and lycopene (b) are short enough to insure efficient photoprotection. Due to larger distances between 800 BChl and lycopene (a) and between *B*850*b* BChl and lycopene (c), these BChl's are not efficiently photoprotected. However, *B*850*b* BChl can transfer excitation energy efficiently to the close *B*850*a* BChl (d).

Here $\hat{z}$ is a unit vector in the direction of the π orbital ($\vec{r}\cdot\hat{z}=r\cos\theta$). The coefficients in (2.35) were determined in [47] as: $a_1=0.008\,47$, $a_2=0.174\,42$, $a_3=0.451\,91$, $a_4=0.436\,45$, $\alpha_1=6.827$, $\alpha_2=2.779$, $\alpha_3=1.625$, and $\alpha_4=1.054$, in atomic units.

To calculate the exchange coupling in Eq. (2.9), we expand the $1s$, $2s$, and $2p\pi$ valence orbitals in terms of Gaussians since the exchange integrals involving Gaussian orbitals can be expressed analytically [48], rendering quick calculations of three- and four-center integrals possible. The H($1s$) and C($2s$) orbitals (of atoms bonded to the conjugated carbons) are expanded in terms of three Gaussians,

$$
\tilde{\phi}'(1s(2s))=\sum_{i=1}^{3}c_i(2\gamma_i/\pi)^{3/4}e^{-\gamma_i r^2}, \tag{2.36}
$$

with coefficients (in a.u.) [48] $c_1=0.444\,635$, $c_2=0.535\,328$, $c_3=0.154\,329$, $\gamma_1=0.168\,856$, $\gamma_2=0.623\,913$, $\gamma_3=3.425\,25$ for the $H(1s)$ orbitals, and $c_1=0.700\,115$, $c_2=0.399\,513$, $c_3=-0.099\,967\,2$, $\gamma_1=0.222\,29$, $\gamma_2=0.683\,482$, $\gamma_3=2.941\,25$ for the C($2s$) orbitals.

The SCF $2p\pi$ orbital (2.35) was approximated by a linear combination of sums of two s orbitals displaced from the

center of the $2p\pi$ orbital by $\pm B_j$ along the axis of the unit vector $\hat{z}$ which accounts for the orientation of the π orbitals 2.37. All π orbitals within one chromophore were taken to be oriented in the same direction. For the carotenoid LYC (with the coordinates of LYC1 in the Protein Data Bank), and BChl's $B850a$, $B850b'$, $B800$, and $B800^*$ employed in our calculations and depicted in Fig. 2, the unit vectors $\hat{z}$ were taken in the x, y, x, z, and z directions of the laboratory frame, respectively. To describe properly the tails of the SCF $2p\pi$ orbitals it is not sufficient to use a linear combination of three $1s$ type Gaussians as for the H($1s$) and C($2s$) orbitals. Instead, the SCF $2p\pi$ orbitals were approximated by means of five $1s$ type Gaussians

$$\tilde{\phi}'(\mathrm{SCF}\,2p\pi)=\sum_{i=1}^{5} b_i(2\beta_i/\pi)^{3/4}(e^{-\beta_i(\vec{r}-B_i\cdot\hat{z})^2} - e^{-\beta_i(\vec{r}+B_i\cdot\hat{z})^2}). \tag{2.37}$$

The coefficients in Eq. (2.37) were determined by a minimization of the χ^2 difference between functions $\tilde{\phi}(\mathrm{SCF}\ 2p\pi)$ as defined in Eq. (2.35) and $\tilde{\phi}'(\mathrm{SCF}\,2p\pi)$ as defined in Eq. (2.37). χ^2 is

$$\chi^2(b_i,\beta_i,B_i)=\sum_r \sum_{\cos\theta} [\tilde{\phi}(\mathrm{SCF}\,2p\pi) - \tilde{\phi}'(\mathrm{SCF}\,2p\pi,b_i,\beta_i,B_i)]^2\Delta r\Delta\cos\theta, \tag{2.38}$$

and is considered on the intervals of 1 a.u. $<r<15$ a.u., $0<\cos\theta<1$. Indices r and $\cos\theta$ indicate that the sums run over a large number of divisions along r and $\cos\theta$ of length Δr and $\Delta\cos\theta$, respectively. The minimization of $\chi^2(b_i,\beta_i,B_i)$ with respect to parameters b_i, β_i, and B_i, yielded the values $b_1=0.354\,20$, $b_2=0.530\,64$, $b_3=0.003\,11$, $b_4=0.000\,15$, $b_5=0.621\,91$, $\beta_1=2.758\,41$, $\beta_2=0.566\,44$, $\beta_3=0.045\,32$, $\beta_4=0.005\,859$, $\beta_5=0.098\,18$, $B_1=0.343\,077$, $B_2=1.627\,830$, $B_3=0.000\,037$, $B_4=0.000\,001$, $B_5=0.597\,397$. The minimization was performed employing a gradient method in 15-parameter space, using the minimization package MINUIT [49].

To check the accuracy of the approximations used to calculate the exchange integrals, we compared the approximated exchange integrals to the exact two-center exchange integrals for Slater orbitals in [50]. For H($1s$) orbitals, the approximated exchange integrals agree within 1% to the values in [50]. The approximated $2p\sigma$ and $2p\pi$ exchange integrals reflect the same distance dependence as the exchange integrals in [50], but are between a factor of 2 and 4 too large. Since various exchange integrals can cancel each other, the factor 2–4 represents an upper bound for the overestimate of the exchange coupling due to the above approximations.

F. Couplings to excitonic states

Electronic excitations in the ring of LH-II's 16 $B850$ BChl's are strongly coupled because of the close proximity of neighboring units (Mg-Mg distance 8.9 or 9.2 Å). Due to this strong coupling, electronic singlet excitations form completely delocalized excitons in the absence of disorder [51]. In our calculations we employ an effective Hamiltonian describing excitons delocalized over the entire ring. This has to be considered an approximation since static and dynamic disorder disrupts the coherency [52]. The suitability of such approximation is further analyzed in the discussion.

An effective Hamiltonian, limited to the Q_y excitations of the individual BChl's, has been constructed and described in [12]. The basis set defining the matrix representation of the effective Hamiltonian contains the elements

$$||\alpha\rangle\rangle=\psi_1(g)\cdots\psi_{\alpha-1}(g)\psi_\alpha(Q_y)\psi_{\alpha+1}(g)\cdots\psi_{2N}(g). \tag{2.39}$$

Here, $\psi_j(g)$ describes the jth BChl in the electronic ground state and $\psi_\alpha(Q_y)$ describes the αth BChl in the Q_y excited state; $2N$ is the number of BChl's in the aggregate, i.e., 16-in case of the $B850$ system of *Rs. molischianum*. Due to pairwise dimerization of BChl's in LH-II, the spectrum of the Hamiltonian displays only an N-fold symmetry, featuring four nondegenerate states ($E_1=11482\ \mathrm{cm}^{-1}$, $E_8=12863\ \mathrm{cm}^{-1}$, $E_9=13715\ \mathrm{cm}^{-1}$, $E_{16}=14046\ \mathrm{cm}^{-1}$) and twelve pairwise degenerate states ($E_{2,3}=11765\ \mathrm{cm}^{-1}$, $E_{4,5}=12250\ \mathrm{cm}^{-1}$, $E_{6,7}=12676\ \mathrm{cm}^{-1}$, $E_{10,11}=13794\ \mathrm{cm}^{-1}$, $E_{12,13}=13922\ \mathrm{cm}^{-1}$, $E_{14,15}=14012\ \mathrm{cm}^{-1}$) [12]. The corresponding eigenstates of this Hamiltonian, the so-called excitonic states (excitons), are represented generically,

$$||n\rangle=\sum_{\alpha=1}^{2N} C_{n\alpha}||\alpha\rangle\rangle. \tag{2.40}$$

Here, $C_{n\alpha}$ are the expansion coefficients as characterized in [12].

Singlet excitation transferred from lycopene (or $B800$ BChl) towards the $B850$ BChl's is not absorbed into electronic excitations of individual BChl's, but into excitonic states. The Coulomb coupling (2.8) between the carotenoid state $|\Psi_{car}\rangle$ and the excitonic state $||n\rangle$ is

$$U_{DA}^c(n)=\sum_\alpha C_{n\alpha}\sum_{i,j,R,S} S_{ij}\frac{e^2}{R_{ijRS}(\alpha)}S_{RS} \times\langle\Psi_D^*|\sum_\sigma c_{i\sigma}^\dagger c_{j\sigma}|\Psi_D\rangle\langle\langle\alpha||\sum_\sigma c_{R\sigma}^\dagger c_{S\sigma}||0\rangle\rangle, \tag{2.41}$$

where $||0\rangle$ represents the electronic ground state of the BChl aggregate.

In case of energetically degenerate exciton states (m_1,m_2), excitation can be absorbed into any linear combination $\cos\gamma||m_1\rangle+\sin\gamma||m_2\rangle$ of these two states. We choose that combination which renders the resulting coupling,

$$U_{DA}^c(m_1,m_2)=\cos\gamma\,U_{DA}^c(m_1)+\sin\gamma\,U_{DA}^c(m_2) \tag{2.42}$$

maximal. This combination is defined through the angle γ specified through

TABLE II. Spectral overlap integrals J_{DA} as defined in Eq. (2.1) in units of eV^{-1} for the states involved in singlet-singlet excitation transfer. Values of J_{DA} smaller than 1×10^{-7} eV^{-1} have been set to zero.

	$2^1A_g^-$	$1^1B_u^+$	Q_y ($B800$)	Q_x ($B800$)
E_1	1.1	7.6×10^{-6}	0.12	0.
$E_{2,3}$	1.4	2.0×10^{-5}	1.2	0
$E_{4,5}$	1.9	1.2×10^{-4}	8.8	0
$E_{6,7}$	2.3	4.7×10^{-4}	7.4	0
E_8	2.4	8.3×10^{-4}	3.9	0
E_9	2.2	8.7×10^{-3}	2.5×10^{-3}	0
$E_{10,11}$	2.2	1.1×10^{-2}	0	0
$E_{12,13}$	2.1	1.5×10^{-2}	0	0
$E_{14,15}$	2.0	1.8×10^{-2}	0	0
E_{16}	2.0	2.0×10^{-2}	0	0
Q_x ($B850$)	6.4×10^{-2}	1.6	0	6.9
Q_x ($B800$)	6.4×10^{-2}	1.6		
Q_y ($B800$)	2.2	2.7×10^{-3}		

$$\tan 2\gamma = \frac{2U^c_{DA}(m_1)U^c_{DA}(m_2)}{U^c_{DA}(m_1)^2 - U^c_{DA}(m_2)^2}. \quad (2.43)$$

In the following we introduce a single index m to enumerate the degenerate states m_1 and m_2 and replace $U_{DA}(m_1,m_2)$ by $U^c_{DA}(m)$. In this manner we will relabel the states such that only one index labels a linear combination [with γ as defined by Eq. (2.43)] of two degenerate states, i.e., we will count subsequently only states with different energy.

The rate of excitation transfer into excitonic state $||n\rangle$ is

$$k_{DA}(n) = \frac{2\pi}{\hbar}|U_{DA}(n)|^2 \int S_D(E)S_{A,n}(E)dE, \quad (2.44)$$

while the total excitation transfer rate is a sum

$$k_{DA} = \sum_n k_{DA}(n). \quad (2.45)$$

G. Spectral overlap integrals

To calculate the spectral overlap integrals in expression (2.1,2.44), $E_{D(A)}$ and $\Gamma_{D(A)}$ for the involved states are needed as parameters. We consider in this regard first the carotenoid- BChl singlet-singlet excitation transfer, with the participating $1^1B_u^+$, $2^1A_g^-$, Q_x and Q_y states. From the absorption spectrum of the LH-II of *Rs. molischianum* reported in [53], one obtains for the Q_x spectrum an E_A value of 590 nm and a Γ_A value of 1240 cm^{-1}, whereas for the Q_y spectrum the width Γ_A is determined to be 460 cm^{-1} [53]. The E_A values of the Q_y exciton states are presented in the previous section. The Γ_A values for the exciton states have been assumed the same as for the Q_y states of individual BChl's, an assumption that is certainly an oversimplification. To describe the emission spectrum of lycopene we employ the available parameters for spheroidene in LH-II of *Rb. sphaeroides* [11], namely, an E_D value of 550 nm and a Γ_D value of 3100 cm^{-1} for the $1^1B_u^+$ state. The use of spheroidene, which has ten conjugated double bonds instead of lycopene, which has 11 conjugated double bonds is justified since small changes in the length of the conjugated systems do not influence the features of the fluorescence spectrum significantly, as shown in [54]. Following the suggestion of [27] for the $2^1A_g^-$ state emission spectrum we assume an equivalence to the emission spectrum of siphonaxanthin in CS_2 [55] and employ an E_D value of 760 nm and a Γ_D value of 3100 cm^{-1}.

Singlet-singlet excitation transfer $B800$ BChl $\rightarrow B850$ BChl can occur either through the Q_x state or through the Q_y state. The absorption spectrum of the $B850$ BChl's is the same as in case of the lycopene$\rightarrow B850$ excitation transfer. The emission spectrum of the Q_y state of the $B800$ band in LH-II of *Rb. sphaeroides* has been measured in [56], with a peak at 805 nm and a width of 230 cm^{-1}. To the best of our knowledge, the emission spectrum of the Q_x state has not been measured in light-harvesting complexes. To characterize the Q_x emission spectrum we assume that the ratio of the widths of the Q_x and Q_y state emission spectra is the same as the ratio for their absorption spectra which yields a Γ_D value of 620 cm^{-1}. We also assume the same shift of the Q_y and Q_x emission maxima compared to their absorption maxima, which leads to an E_D value of 595 nm for the Q_x state of $B800$ BChl.

The spectral overlap integrals for the various singlet-singlet excitation transfers are listed in Table II. For triplet-triplet excitation transfer we assume a spectral overlap integral of 1 eV^{-1} as suggested in [27].

III. RESULTS

The atomic level structure of LH-II of *Rs. molischianum* revealed the relative arrangement of lycopenes and BChl's in the protein; this permitted us to determine the Coulomb (2.26) and exchange (2.29) coupling and the associated rates of excitation transfer. Below we present the transition density matrix elements for the lycopene and BChl analogue employed in the calculations and the electronic couplings and rates for different transfer pathways.

A. Transition density matrix elements

Figure 6 shows the transition density matrix elements ${}^0\tilde{M}_D(i,j) + {}^0\tilde{M}_D(j,i)$ $(i \neq j)$ and ${}^0\tilde{M}_A(i,i)$ for the caro-

tenoid $1^1B_u^+$ and $2^1A_g^-$ states as calculated from expressions (2.27,2.28), i.e., employing the nonorthogonal atomic orbitals. The transition density matrix elements ${}^0M_D(i,j)+{}^0M_D(j,i)$ $(i\neq j)$ and ${}^0M_A(i,i)$ [Eqs. (2.19,2.20)] expressed in terms of orthogonal orbitals are shown in brackets. The alternancy symmetry of polyenes is reflected in the vanishing ${}^0M_D(i,j)+{}^0M_D(j,i)$ values for the $1^1B_u^+ \rightarrow 2^1A_g^-$ transition for bonds $(j=i\pm 1)$ and those of the $2^1A_g^- \rightarrow 1^1A_g^-$ transition in the vanishing ${}^0M_D(i,i)$ values. The observed selection rules are derived in the Appendix. The slight deviation of positions of lycopene C atoms from those of perfect polyenes is not destroying the alternancy symmetry, since this deviation concerns only the off-diagonal matrix elements of the PPP Hamiltonian. A change in the diagonal elements, i.e., ionization potentials of C atoms, would, however, result in disruption of alternancy symmetry.

Figure 7 shows the transition density matrix elements ${}^0\tilde{M}_A(R,S)+{}^0\tilde{M}_A(S,R)$ $(R\neq S)$ and ${}^0\tilde{M}_A(R,R)$ for the BChl $Q_x\rightarrow$ ground state and $Q_y\rightarrow$ ground state transitions as calculated from expression (2.28) for the symmetric BChl analogue (cf. Fig. 5).

The transition density matrix elements for the BChl and carotenoid triplet $\rightarrow$ ground state transitions are shown in Fig. 8.

B. Transition Dipole Moments

Expression (2.26) with the Coulomb integrals $(\tilde{\phi}_i\tilde{\phi}_j|\tilde{\phi}_R\tilde{\phi}_S)$ given by Eq. (2.31) can be expanded into a multipole series,

$$\begin{aligned}U^c_{DA}=&\frac{c_Ac_D}{|\vec{R}_D-\vec{R}_A|}-\frac{\vec{R}_D-\vec{R}_A}{|\vec{R}_D-\vec{R}_A|^3}\cdot(c_A\vec{d}_D-c_D\vec{d}_A)\\&+\frac{3}{2|\vec{R}_D-\vec{R}_A|^5}\{c_A[\vec{d}_D\cdot(\vec{R}_D-\vec{R}_A)]^2\\&-2[\vec{d}_D\cdot(\vec{R}_D-\vec{R}_A)][\vec{d}_A\cdot(\vec{R}_D-\vec{R}_A)]\\&+c_D[\vec{d}_A\cdot(\vec{R}_D-\vec{R}_A)]^2\}-\frac{1}{2|\vec{R}_D-\vec{R}_A|^3}[(c_A|\vec{d}_D|^2)\\&-2\vec{d}_D\cdot\vec{d}_A+(c_D|\vec{d}_A|^2)]+\mathrm{O}\left(\frac{1}{|\vec{R}_D-\vec{R}_A|^4}\right)\end{aligned}\tag{3.1}$$

which converges rapidly for $|\vec{r}_{ij}-\vec{r}_{RS}|\ll|\vec{R}_D-\vec{R}_A|$. Here $\vec{R}_D$ and $\vec{R}_A$ are centers of mass of the donor and acceptor molecules, respectively, and r_{ij} (r_{RS}) are distances of midpoints of atoms $i(R)$ and $j(S)$ from $\vec{R}_D$ $(\vec{R}_A)$; c_D and c_A are the monopole moments of donor and acceptor defined through

$$c_D=\sqrt{2}e\sum_{i,j}S_{ij}\tilde{M}_D(i,j),\tag{3.2}$$

$$c_A=\sqrt{2}e\sum_{R,S}S_{RS}\tilde{M}_A(R,S),\tag{3.3}$$

and $\vec{d}_D$ and $\vec{d}_A$ are the respective dipole moments,

$$\vec{d}_D=\sqrt{2}e\sum_{i,j}\vec{r}_{ij}S_{ij}\tilde{M}_D(i,j),\tag{3.4}$$

$$\vec{d}_A=\sqrt{2}e\sum_{R,S}\vec{r}_{RS}S_{RS}\tilde{M}_A(R,S).\tag{3.5}$$

Employing Eqs. (2.27,2.28) one can verify

$$c_D=\sqrt{2}e\sum_i M_D(i,i)\tag{3.6}$$

and, using Eq. (2.12) together with $\mathbb{1}=\Sigma_{i,\sigma}c^\dagger_{i\sigma}c_{i\sigma}$ and the orthogonality of $|\Psi^*_D\rangle,|\Psi_D\rangle$, one can show that the monopole c_D vanishes. The same holds for c_A. This property of c_D and c_A is expected and implies that the leading term of the multipole expansion (3.1) is the dipole-dipole term, i.e., the third and fourth terms in Eq. (3.1). We note that only the consistent use of nonorthogonal atomic orbitals in calculating U^c_{DA} reproduces this result; if one employs a combination of $(\tilde{\phi}_i\tilde{\phi}_j|\tilde{\phi}_R\tilde{\phi}_S)$ with transition density matrix elements $M_D(i,j)$ and $M_A(R,S)$ rather than $\tilde{M}_D(i,j)$ and $\tilde{M}_A(R,S)$, the monopole terms do not necessarily vanish and grave errors result.

In a similar fashion one can derive using Eqs. (2.27) and notation $\vec{r}_{ii}=\vec{r}_i$,

$$\vec{d}_D=\sum_i e\vec{r}_iM_D(i,i),\tag{3.7}$$

which in turn is equal to the well-known expression for the transition dipole moment,

$$\vec{d}_D=\langle\Psi^*_D|\sum_i e\vec{r}_i|\Psi_D\rangle,\tag{3.8}$$

where $\vec{r}_i$ is the position of atom i. One can derive an equivalent result for $\vec{d}_A$ as defined in Eq. (3.5).

The calculated transition dipole moments of the different electronic states of lycopene and BChl's in LH-II *Rs. molischianum* are shown in Table III. As expected, the $2^1A_g^-$ state dipole moment vanishes within the precision limited by errors in the atomic coordinates. The calculated transition dipole moment of $1^1B_u^+$ agrees well with the experimental value of 13 Debye [57]. The value of the transition dipole moment of Q_x agrees also remarkably well with the experimental value of 3.29 D; however, the calculated value of the transition dipole moment of Q_y exceeds the measured value of 6.13 D [58] by more than a factor of 2.

C. Lycopene-BChl singlet excitation transfer

Table IV provides the coupling terms $U^{ex,c}_{DA}$ and associated transfer rates for the $1^1B_u^+\rightarrow Q_x$ and $2^1A_g^-\rightarrow Q_y$ excitation transfer from lycopene to different BChl's (shown in Fig. 2). We consider only coupling of the LYC_{down} to the $B850$ BChl's and of LYC_{up} to the $B800$ BChl's. $1^1B_u^+ \rightarrow Q_y$ and $2^1A_g^-\rightarrow Q_x$ excitation transfers are not considered since the rates are negligible due to small spectral overlap (Table II).

TABLE III. Transition dipole moments in Debye for subunit one of LH-II of *Rs. molischianum*, calculated according to Eqs. (3.4, 3.5). In case of lycopene we present the results for LYC_{down} only.

Pigment (state)	d_x	d_y	d_z	$\lvert\vec{d}\rvert$
LYC ($2^1A_g^-$)	−0.002	0.001	0.000	0.002
LYC ($1^1B_u^+$)	2.577	10.598	−10.444	15.101
*B*850*a* (Q_y)	−13.777	−1.838	−3.771	14.402
*B*850*a* (Q_x)	0.006	−0.145	−3.383	3.386
*B*850*b* (Q_y)	12.972	4.686	−3.896	14.332
*B*850*b* (Q_x)	0.073	−0.242	−3.396	3.406
*B*800 (Q_y)	10.738	9.282	−2.117	14.351
*B*800 (Q_x)	−0.905	2.793	1.712	3.399

The exchange couplings between lycopene and its closest four BChl's have been calculated according to expression (2.29), (with $l=0$) and the Coulomb couplings according to expression (2.26). The transfer rates for the exchange and the Coulomb coupling have been determined then from expression (2.1) assuming that the coupling U_{DA} is either only due to exchange coupling ($U_{DA}=U_{DA}^{ex}$) or only due to Coulomb coupling ($U_{DA}=U_{DA}^{c}$) and using the spectral overlap integrals listed in Table II.

Because of the excitonic nature of the *B*850 Q_y band, the transfer rates for Coulomb coupling to the *B*850 Q_y band have also been calculated according to expression (2.45). Table V lists the couplings between lycopene $1^1B_u^+$ and $2^1A_g^-$ states and the individual excitonic states as evaluated according to expressions (2.41-2.43) using the spectral overlap integrals listed in Table II. The transfer rates to the Q_y exciton band are given by the sum of the transfer rates to the individual exciton states (2.44) and are provided in Tables IV and V.

The largest rates are found for transfer from the $1^1B_u^+$ state to the Q_x band through the Coulomb mechanism. The most strongly coupled BChl's are *B*850*a*′ and *B*800* BChl, the two BChl's positioned closest to the lycopene.

The $2^1A_g^- \rightarrow Q_y$ pathway, is more than 100 times slower than the $1^1B_u^+ \rightarrow Q_x$ pathway with the excitonic structure of the Q_y band speeding up the rate of excitation transfer only slightly.

The transfer rates through exchange coupling for the $1^1B_u^+ \rightarrow Q_x$ pathway are predicted at least six orders of magnitude smaller than those through Coulomb coupling.

D. *B*800 BChl-*B*850 BChl singlet excitation transfer

Table VI provides the coupling energies U_{DA}^c and associated transfer rates for the different possible pathways from *B*800 BChl to its closest *B*850 BChl. The couplings and rates were calculated as for lycopene-*B*850 BChl coupling, except that the donor states were given by the *B*800 BChl Q_y and

TABLE IV. Couplings (in eV) and transfer rates (in Hz) for the $1^1B_u^+$-Q_x and $2^1A_g^-$-Q_y excitation transfer pathways from lycopene (LYC) to different BChl's (shown in Fig. 2). The couplings are calculated according to Eqs. (2.26,2.29). The rates are calculated according to Eq. (2.1) assuming that the coupling U_{DA} is either only due to exchange coupling $U_{DA}=U_{DA}^{ex}$ or only due to Coulomb coupling $U_{DA}=U_{DA}^{c}$. Because of the excitonic nature of the *B*850 Q_y band, the transfer rates through Coulomb coupling are also calculated according to Eqs. (2.42–2.45). The corresponding couplings to the different exciton states are listed in Table V.

	$1^1B_u^+$-Q_x		$2^1A_g^-$-Q_y	
BChl	$\lvert U_{DA}^c\rvert$	$k(U_{DA}^c)$	$\lvert U_{DA}^c\rvert$	$k(U_{DA}^c)$
*B*850*a*	2.2×10^{-3}	7.3×10^{10}	1.6×10^{-4}	3.4×10^{8}
*B*850*b*	5.4×10^{-3}	4.4×10^{11}	2.9×10^{-5}	1.1×10^{7}
*B*850*a*′	1.8×10^{-2}	4.8×10^{12}	4.7×10^{-4}	3.0×10^{9}
*B*850*b*′	5.8×10^{-3}	5.1×10^{11}	2.4×10^{-5}	7.6×10^{6}
Exciton			see Table V	4.9×10^{9}
*B*800*	1.6×10^{-2}	4.0×10^{12}	2.1×10^{-4}	9.0×10^{8}
*B*800	2.8×10^{-3}	1.2×10^{11}	3.7×10^{-5}	2.8×10^{7}
BChl	$\lvert U_{DA}^{ex}\rvert$	$k(U_{DA}^{ex})$	$\lvert U_{DA}^{ex}\rvert$	$k(U_{DA}^{ex})$
*B*850*b*	1.4×10^{-10}	3.2×10^{-4}	4.1×10^{-10}	2.2×10^{-3}
*B*850*a*′	2.9×10^{-6}	1.3×10^{5}	4.5×10^{-6}	2.8×10^{5}
*B*800*	6.8×10^{-8}	7.0×10^{1}	7.3×10^{-8}	1.1×10^{2}
*B*800	2.2×10^{-9}	7.7×10^{-2}	1.8×10^{-9}	6.5×10^{-2}

TABLE V. Coulomb couplings (in eV) and transfer rates (in Hz) between the singlet lycopene states and the exciton states of the $B850$ BChl Q_y band.

Exciton State	$\lvert U^c_{DA}\rvert$ $(2^1A_g^-)$	$k(U^c_{DA})$ $(2^1A_g^-)$	$\lvert U^c_{DA}\rvert$ $(1^1B_u^+)$	$k(U^c_{DA})$ $(1^1B_u^+)$
E_1	7.1×10^{-5}	5.8×10^{6}	1.8×10^{-2}	2.3×10^{7}
$E_{2,3}$	1.3×10^{-4}	2.2×10^{8}	2.0×10^{-2}	7.7×10^{7}
$E_{4,5}$	1.7×10^{-4}	5.5×10^{8}	2.2×10^{-2}	5.8×10^{8}
$E_{6,7}$	2.0×10^{-4}	8.5×10^{8}	2.3×10^{-2}	2.4×10^{9}
E_8	1.4×10^{-4}	4.2×10^{8}	1.6×10^{-2}	2.0×10^{9}
E_9	1.8×10^{-4}	6.8×10^{8}	6.4×10^{-3}	3.4×10^{9}
$E_{10,11}$	2.3×10^{-4}	10.9×10^{8}	8.6×10^{-3}	7.7×10^{9}
$E_{12,13}$	1.8×10^{-4}	6.3×10^{8}	7.4×10^{-3}	7.8×10^{9}
$E_{14,15}$	1.3×10^{-4}	3.4×10^{8}	7.4×10^{-3}	7.8×10^{9}
E_{16}	8.3×10^{-5}	1.3×10^{8}	1.9×10^{-3}	7.0×10^{8}
Σ		4.9×10^{9}		3.2×10^{10}

Q_x states, instead of the lycopene $1^1B_u^+$ and $2^1A_g^-$ states. The couplings between $B800$ and $B850$ BChl's are listed in Table VI. Couplings between states that are not listed are negligible.

Besides the couplings to individual $B850$ BChl states also the couplings to the different exciton states of the $B850$ BChl Q_y band are listed in Table VI. The rate for transfer to the exciton band, given as the sum of the transfer rates to the different exciton states, is ten times faster then the transfer rates for transfer to an individual $B850$ BChl. Exchange coupling has not been investigated since $B800$ and $B850$ BChl's, with a closest Mg-Mg distance of 19 Å, are out of range of the Dexter mechanism.

E. Triplet excitation transfer

Table VII provides the coupling energies U^{ex}_{DA} and associated transfer rates, calculated according to Eqs. (2.29) (l $=1$), and (2.1), for triplet excitation transfer from three BChl's ($B800$, $B850a$, $B850b$, cf. Fig. 2) to the closest lycopene (LYC). $B850a$ BChl transfers triplet excitation energy to this lycopene within 0.7 μs while transfer from $B850b$ and $B800$ BChl's to lycopene are, respectively, eleven and six orders of magnitude slower. However, $B850b$ BChl can transfer triplet excitation energy to its closest $B850a$ BChl within 3.5 ns making indirect transfer possible.

TABLE VI. Coulomb couplings (in eV) and transfer rates (in Hz) for the different singlet-singlet excitation transfer pathways from $B800$ BChl to $B850$ BChl. Only couplings between $B800$ BChl and the $B850$ BChl to which the former is most strongly coupled are listed (upper part of the Table).

States	$\lvert U^c_{DA}\rvert$	$k(U^c_{DA})$
Q_y ($B800$)-Q_y ($B850a'$)	1.6×10^{-2}	2.9×10^{12}
Q_x($B800$)-Q_y ($B850a$)	2.3×10^{-3}	0
Q_y ($B800$)-Q_x ($B850a$)	2.6×10^{-3}	0
Q_x ($B800$)-Q_x ($B850b$)	5.3×10^{-4}	1.8×10^{10}
Q_y ($B800$)-E_1	2.7×10^{-3}	8.2×10^{9}
Q_y ($B800$)-$E_{2,3}$	8.7×10^{-3}	8.6×10^{11}
Q_y ($B800$)-$E_{4,5}$	1.0×10^{-2}	8.8×10^{12}
Q_y ($B800$)-$E_{6,7}$	7.4×10^{-3}	3.8×10^{12}
Q_y ($B800$)-E_8	2.4×10^{-3}	2.2×10^{11}
Q_y ($B800$)-Q_y ($B850$-exciton)		13.7×10^{12}

IV. DISCUSSION

Excitation energy in photosynthetic light harvesting flows primarily in the form of chlorophyll Q_y excitations at near-infrared energies. The carotenoids fuel this stream with photons absorbed in the middle of the visible spectrum and employ for that purpose a short lived, but strongly allowed $1^1B_u^+$ state and a low-lying optically forbidden $2^1A_g^-$ state. The exact contribution of the two states to the excitation transfer and the mechanism of excitation transfer are subject of debate with different mechanisms and pathways being proposed in the literature (see, e.g., [12,20,30,59,60]).

The calculations in this paper predict that, for the case of LH-II of *Rs. molischianum*, the singlet excitation transfer proceeds through the Coulomb and not the electron exchange mechanism. For all excitation transfer pathways (Table IV) the Coulomb coupling exceeds the electron exchange coupling by a factor of 100 [$2^1A_g^- \rightarrow Q_y$ ($B850a'$) transfer] to up to 10^7[$1^1B_u^+ \rightarrow Q_x$ ($B850b$) transfer], which means that transfer rates through Coulomb coupling exceed transfer rates through exchange coupling by at least four orders of magnitude.

Due to vibrations of the protein the positions of the chromophores can change. Since a distance change affects the exchange coupling stronger than the Coulomb coupling, one might argue that the exchange coupling can become stronger than the Coulomb coupling for shorter distances. To estimate

TABLE VII. Exchange couplings (in eV) and transfer rates (in Hz) for the triplet-triplet excitation transfers from BChl to lycopene and from $B850b$ BChl to $B850a'$ BChl.

BChl	$\lvert U^{ex}_{DA}\rvert$	$k(U^{ex}_{DA})$
$B850a'$	1.2×10^{-5}	1.4×10^{6}
$B850b$	6.2×10^{-11}	3.6×10^{-5}
$B800$	2.7×10^{-8}	7.0
$B850b\rightarrow B850a$	1.7×10^{-4}	2.9×10^{8}

the effect of position changes on the couplings, we have shifted the position of the BChl's along the axis connecting the centers of mass of BChl's and lycopene and calculated the ratio between Coulomb and exchange coupling. Even after a rather dramatic shift of 3 Å, the Coulomb coupling still exceeds the exchange coupling by a factor of 3 ($2^1A_g^- \rightarrow Q_y$ ($B850a'$) transfer) to 1500 [$1^1B_u^+ \rightarrow Q_x$ ($B850b$) transfer]. Since in our calculations the exchange coupling has been overestimated by up to a factor of 4 due to the use of Gaussian orbitals, one can conclude safely that carotenoid-bacteriochlorophyll singlet excitation transfer proceeds through the Coulomb and not the Dexter mechanism.

Of the different possible pathways from lycopene to $B850$ BChl only the $1^1B_u^+ \rightarrow Q_x$ pathway furnishes a subpicosecond transfer time, proceeding within 210 fs from lycopene to the closest $B850$ BChl. Adding up the rates for other transfer channels, especially lycopene $\rightarrow B800$ transfer, results in a time of 115 fs for excitation transfer from the $1^1B_u^+$ state through all possible transfer pathways. This time is in good agreement with the above-mentioned reduction of the $1^1B_u^+$ state lifetime from 200 fs in organic solvent to 80 fs in LH-II which suggests a transfer time of 135 fs. Likewise, the experimentally determined lifetime reduction of the $2^1A_g^-$ state from 9.1 ps in organic solvent to about 2 ps in LH-II corresponds to a transfer time of 2.5 ps. However, the calculated time of 330 ps (Table IV) for $2^1A_g^- \rightarrow Q_y$ transfer between lycopene and $B850a'$ BChl differs from the experimental value estimated from the lifetime by two orders of magnitude.

Improvement of the theoretical treatment of the $2^1A_g^-$ state is needed for understanding excitation transfer involving this state. The present description assumes that the state is completely optically forbidden. However, the finite radiative lifetime $\tau_r = 2$ μs [20] of the $2^1A_g^-$ state in β-carotene implies that the $2^1A_g^-$ state borrows intensity from the optically allowed $1^1B_u^+$ state. The mechanism of intensity borrowing involves higher vibrational levels of the $2^1A_g^-$ state. Indeed, several stretching modes of the lycopene $2^1A_g^{-1}$ state exhibit vibrational relaxation on a time scale slower than that of internal conversion to the ground state [61], suggesting that these modes are responsible for excitation transfer from the $2^1A_g^-$ state. Intensity borrowing for the $2^1A_g^-$ can be enhanced through the methyl groups attached to the conjugated system of lycopene (see Fig. 5) that are not accounted for in the Hamiltonian [Eq. (2.21)] and that break the alternancy symmetry of the π-electron system.

Intensity borrowing speeds up $2^1A_g^- \rightarrow Q_y$ excitation transfer; future theoretical studies including the above-mentioned effects of intensity borrowing through vibrational modes or symmetry breaking will have to determine whether the $2^1A_g^- \rightarrow Q_y$ transfer time can be as short as the 2.5 ps estimated from the lifetime.

Since bacteriochlorophyll Q_y excitations in the $B850$ system are strongly coupled, the respective absorbing states are exciton states. Transfer from the $2^1A_g^-$ state to exciton states is slightly faster than the transfer $2^1A_g^- \rightarrow$ individual BChl Q_y state, proceeding within 200 ps (Table V). This effect is due to the spreading of the exciton energies over a 871 nm to 712 nm range (Fig. 3), which improves the overlap between donor and acceptor states. The $1^1B_u \rightarrow Q_x$ transfer time is essentially unaffected by exciton splitting which measures only a few cm^{-1} for the Q_x state [51].

It is debatable whether the picture of excitation delocalized over the entire ring is correct, since thermal disorder disrupts the coherency of the exciton states [52]. No consensus has yet been reached about the length of exciton delocalization i.e., the number of coherently coupled BChl's; estimates ranging from two BChl molecules [62] to almost the entire length of the $B850$ BChl aggregate [63]. Future calculations should take the effect of static and dynamic disorder on the enhancement of the transfer rate due to exciton splitting into account; respective descriptions pose still a conceptual and practical challenge.

In addition to the direct transfer pathways from lycopene to the $B850$ BChl's, singlet excitation transfer to the $B850$ BChl's can also occur via the lycopene $1^1B_u^+ \rightarrow B800^*$ Q_x route with a transfer time of 250 fs (Table IV). The $B800$ Q_x state relaxes within 200 fs into the Q_y state from which excitation energy can be transferred on to the $B850$ BChl ring.

As in the case of the lycopene $\rightarrow B850$ BChl pathway, $B800$ Q_y states couple to the $B850$ exciton states rather than to individual BChl's. The strongest coupling ($U_{DA}^c = 1.0 \times 10^{-2}$ eV) is to the $E_{4,5}$ energy levels and not to the $E_{2,3}$ energy levels ($U_{DA}^c = 8.7 \times 10^{-3}$ eV) as revealed by Table VI, even though the latter states are the only strongly optically allowed states, i.e., carry the strongest transition dipole moments. However, a $B800$ BChl interacts stronger with closer $B850$ BChl's and thus breaks the ring symmetry; the latter is crucial since the dipole forbidden character of the exciton states needs to be overcome.

The effect of the excitonic structure of the $B850$ Q_y band is to shorten the transfer time between $B800$ and $B850$ Q_y states due to improved spectral overlap; neglecting the exciton splitting results in a time of 350 fs for transfer between a $B800$ and its closest $B850$ Q_y state; the inclusion of the splitting reduces the transfer time to 73 fs as shown in Table VI. This is too short compared to the experimentally measured transfer time of 700 fs [11]. However, the calculated dipole moments (14.4 D) of the Q_y state are significantly larger than the experimental values (6.13 D) as pointed out above. This error is due to the inaccuracy in the employed wave function and can be reduced through more extensive electronic structure calculations. The $B800$–$B850$ coupling is mostly due to dipolar coupling, and one could use the ratio of calculated to experimental oscillator strength to scale the coupling; this would lead to a time of 10.2 ps for excitation transfer between individual $B800$ and $B850$ BChl's and 2.2 ps for transfer from $B800$ to the $B850$ exciton band.

The role of exciton splitting and spectral overlap in enhancing $B800$ to $B850$ energy transfer can be readily reconstructed from Tables II, VI and Eqs. (2.44,2.45). For example, transfer from the $B800$ Q_y state to the $E_{4,5}$ levels has a spectral overlap of 8.8 eV^{-1}, whereas the overlap to the $E_{2,3}$ levels is only 1.2 eV^{-1}, i.e., the spectral overlap favors the $E_{4,5}$ exciton states. An error in the evaluation of the spectral overlap results from the extremely simplifying approximation of the spectra by Gaussians as well as from an overestimate of the extent of exciton delocalization. This error, in

addition to the erroneously large value of transition dipole moments, can account for the difference between calculated and experimental transfer times.

Triplet excitation transfer through the Dexter mechanism is highly sensitive to the atomic distances between the donor and acceptor moieties. Figure 9 shows the region of closest contact between BChl's and carotenoids in LH-II of *Rs. molischianum*. The conjugated π-electron systems of *B*850*b* BChl and *B*800 BChl exhibit a larger distance to the conjugated π-electron system of lycopene than to that of *B*850*a* BChl. The distances between the conjugated atoms of lycopenes and BChl's determine the transfer times; the effect of nonconjugated carbon and hydrogen bridge atoms [see Fig. 9(a)] on the overall transfer time is small.

Our calculations predict times of 0.7 μs for *B*850*a*′ BChl $\rightarrow$ lycopene triplet excitation transfer (see Fig. 9). Given the BChl triplet state lifetime of 10 μs one can expect a high efficiency of quenching of the *B*850*a* BChl triplet states. In contrast, the calculated transfer times for *B*800 BChl $\rightarrow$ lycopene and *B*850*b* BChl $\rightarrow$ lycopene transfer are too long to ensure an efficient photoprotection by the lycopene shown in Figs. 2,9. Our calculations suggest an indirect photoprotection mechanism for *B*850*b* BChl. *B*850*b* BChl can transfer triplet excitation within 3.5 ns to its closest *B*850*a* BChl which is efficiently protected by the lycopene. The motif that BChl's are protected indirectly has been found also in the RC [64] and in the light harvesting complex LHC-II of plants [65].

Our results indicate that *B*800 BChl's are not photoprotected. It has been suggested on account of biochemical observation [53] that a second set of eight lycopenes exists in LH-II of *Rs. molischianum* which are not resolved in the x-ray structure. It is possible that photoprotection of all the BChl's in LH-II of *Rs. molischianum* involves this set of lycopenes, which have yet to be resolved through x-ray scattering. However, a recent stoichiometric analysis contradicts this observation and suggests that only one set of lycopenes exists in LH-II [66]. Alternatively, it might be possible that the fast singlet excitation transfer (within less than a picosecond) from *B*800 BChl's to the *B*850 BChl ring is so efficient that the *B*800 BChl's do not require photoprotection. A third explanation is that while the *B*800 BChl's do not appear to be protected for the geometry of the static crystal structure, they may be found protected once fluctuations, which bring the *B*800 BChl into closer contact with lycopene, are taken into account. According to our calculations the *B*800 BChl's has to move about 1.75 Å in the direction of the axis connecting its own center of mass with that of lycopene to become significantly protected. A molecular dynamics or resonance Raman study may reveal whether such movements can occur within a few μs.

ACKNOWLEDGMENTS

The authors would like to thank Xiche Hu, Lubos Mitas, and Petar Maksimović for useful discussions, as well as Michael Zerner for a communication of the data. We acknowledge financial support from the National Science Foundation (Grant Nos. NSF BIR 94-23827 EQ and NSF BIR 9318159), the National Institutes of Health (Grant No. NIH PHS 5 P41 RR05969-04), and the Carver Charitable Trust.

FIG. 10. Starred and unstarred atoms in $C_{10}H_{12}$.

APPENDIX: ALTERNANCY SYMMETRY SELECTION RULES

This section derives selection rules for the matrix elements (2.19,2.20) of the transition operators ${}^{km}\hat{O}_j^i$ based on the alternancy symmetry displayed by the PPP Hamiltonian for alternant hydrocarbons [67–69].

The alternancy symmetry results from a topological feature of alternant hydrocarbons, according to which it is possible to divide unsaturated carbon atoms into two sets, ''starred'' (C^*) and ''unstarred'' (C°) atoms, such that no two atoms of a set are joined by a bond. Figure 10 shows the ''starred'' and ''unstarred'' atoms in polyene $C_{10}H_{12}$. The orthogonal π-atomic orbitals of the ''starred'' and ''unstarred'' atoms will be labeled $|*,\nu\rangle$ and $|\bigcirc,\nu\rangle$, respectively.

1. One-electron pairing properties

The alternancy symmetry is responsible for the one-electron pairing properties of alternant hydrocarbons, i.e., molecular orbital energies occur in pairs, ϵ_n and $-\epsilon_n+\epsilon$, where ϵ is the same constant for all molecular orbitals. The corresponding wave functions are

$$|\Psi_n\rangle=\sum_\nu^N (C_{n\bigcirc\nu}|\bigcirc,\nu\rangle+C_{n*\nu}|*,\nu\rangle), \tag{A1}$$

$$|\tilde{\Psi}_n\rangle=\sum_\nu^N (C_{n\bigcirc\nu}|\bigcirc,\nu\rangle-C_{n*\nu}|*,\nu\rangle), \tag{A2}$$

respectively, for ϵ_n and $-\epsilon_n+\epsilon$. The molecular orbital $|\tilde{\Psi}_n\rangle$ is termed ''alternantly conjugate'' to $|\Psi_n\rangle$. The alternantly conjugate orbital to the spin molecular orbital $|\Psi_{n\eta}\rangle=|\Psi_n\rangle|\eta\rangle$, $\eta=\alpha,\beta$, is defined such that the spin state is unaltered by the alternancy conjugation, i.e., $|\tilde{\Psi}_{n\eta}\rangle=|\tilde{\Psi}_n\rangle|\eta\rangle$ [67]. $|\tilde{\Psi}_n\rangle$ is related to $|\Psi_n\rangle$ through the alternation operator $\hat{B}$,

$$|\tilde{\Psi}_n\rangle=\hat{B}|\Psi_n\rangle, \tag{A3}$$

which, according to Eqs. (A1,A2), is

$$\hat{B}=\hat{L}_\bigcirc-\hat{L}_*. \tag{A4}$$

Here $L_\bigcirc$ and L_* are the projection operators for the two spaces spanned by the unstarred and the starred π atomic orbitals, i.e.,

$$\hat{L}_{\bigcirc}=\sum_{\nu}|\bigcirc,\nu\rangle\langle\bigcirc,\nu|,\quad \hat{L}_{*}=\sum_{\nu}|*,\nu\rangle\langle*,\nu|, \quad \text{(A5)}$$

that satisfy

$$\hat{L}_{\bigcirc}+\hat{L}_{*}=\hat{I},\quad \hat{L}_{\bigcirc}\hat{L}_{*}=\hat{0}. \quad \text{(A6)}$$

Operator $\hat{B}$ and its Hermitian conjugate $\hat{B}^{\dagger}$ obey the unitarity condition

$$\hat{B}^{\dagger}\hat{B}=\hat{B}^{2}=\hat{I} \quad \text{(A7)}$$

such that the eigenvalues of $\hat{B}$ are ± 1.

2. *N*-electron pairing properties

The one-electron pairing properties can be generalized readily to *N*-electron systems. In each of the one-electron vector spaces that span the *N*-electron space, the alternation operator is defined as

$$\hat{B}(k)=\hat{L}_{\bigcirc}(k)-\hat{L}_{*}(k),\quad k=1,\ldots,N \quad \text{(A8)}$$

where the index k labels an electron. Operator $\hat{B}(k)$ satisfies properties (A6,A7). Operator $\hat{B}_N$, acting on an *N*-electron wave function, is a product of the one-electron alternation operators $\hat{B}(k)$, namely,

$$\hat{B}_N=\prod_{k=1}^{N}\hat{B}(k). \quad \text{(A9)}$$

The pairing operator acting in the Fock space of N electrons is defined through [68]

$$\hat{P}=\hat{B}_N\hat{D}, \quad \text{(A10)}$$

where

$$\hat{D}=\sum_{p}\mathrm{sgn}(p)p\prod_{i=1}^{N}a^{\dagger}_{p_k}(i)\prod_{j=N+1}^{2N}a_{p_{k'}}(j). \quad \text{(A11)}$$

and where p is a permutation between electron spin orbitals, as denoted by

$$p=\begin{pmatrix}1, & \cdots, & N, & N+1, & \cdots, & 2N\\ p_1, & \cdots, & p_N, & p_{N+1}, & \cdots, & p_{2N}\end{pmatrix}. \quad \text{(A12)}$$

We define $\mathrm{sgn}(p)=\pm 1$ for even /odd permutations p. Indices i and j label the electrons, the p_k's label molecular spin orbitals. $a^{\dagger}_{p_k}$ and $a_{p'_k}$ create and annihilate, respectively, an electron in spin orbitals p_k and $p_{k'}$.

The commutation relation of the PPP Hamiltonian for alternant hydrocarbons and the pairing operator $\hat{P}$ is [68,67]

$$\hat{H}\hat{P}-\hat{P}\hat{H}=2\epsilon\hat{P}, \quad \text{(A13)}$$

where ϵ is a scalar. The commutation property implies that eigenvectors of $\hat{H}$ are also eigenvectors of $\hat{P}$. Operator $\hat{P}$ is unitary, i.e.,

$$\hat{P}^{\dagger}\hat{P}=\hat{P}^{2}=\hat{I}, \quad \text{(A14)}$$

and, hence, its eigenvalues are ± 1, i.e.,

$$\hat{P}|x\rangle=\pm|x\rangle. \quad \text{(A15)}$$

The alternancy symmetry of the polyene states involved in our calculations is $1^1A_g^-$, $2^1A_g^-$ and $1^3B_u^+$, ''+'' and ''−'' states being the eigenstates of $\hat{P}$ with eigenvalues $+1$ and -1, respectively [67].

3. Transformation of couplings under alternancy conjugation

The matrix elements between the eigenstates of $\hat{P}$, $|x\rangle$ and $|y\rangle$, for a one-electron Hermitian operator $\hat{A}$, obey

$$\langle x|\hat{A}|y\rangle=\pm\langle x|\hat{P}^{\dagger}\hat{A}\hat{P}|y\rangle. \quad \text{(A16)}$$

If the states $|x\rangle$ and $|y\rangle$ are the eigenstates of $\hat{P}$ for the same eigenvalue, the upper sign applies in Eq. (A16), otherwise, the lower sign applies. According to definition (A10) we express, following [68],

$$\hat{P}^{\dagger}\hat{A}\hat{P}=\hat{D}^{\dagger}\hat{B}_N^{\dagger}\hat{A}\hat{B}_N\hat{D}. \quad \text{(A17)}$$

$\hat{B}_N^{\dagger}$ and $\hat{D}^{\dagger}$ are the Hermitian conjugates of $\hat{B}_N$ and $\hat{D}$, respectively.

An arbitrary operator $\hat{C}$ can be written

$$\hat{C}=\hat{C}_{+}+\hat{C}_{-}, \quad \text{(A18)}$$

where

$$\hat{C}_{+}=\sum_{i=\bigcirc,*}\hat{L}_i\hat{C}\hat{L}_i\quad \hat{C}_{-}=\sum_{\substack{i,j=\bigcirc,*\\ i\neq j}}\hat{L}_i\hat{C}\hat{L}_j, \quad \text{(A19)}$$

operators $L_{\bigcirc}$ and L_{*} being defined in Eq. (A5). For a one-electron operator (acting on electron k) holds

$$\hat{B}_N^{\dagger}\hat{A}(k)\hat{B}_N=\hat{B}(k)^{\dagger}\hat{A}(k)\hat{B}(k), \quad \text{(A20)}$$

since $\hat{A}(k)$ acts as an identity operator on all electrons, except electron k. Due to Eq. (A7) the problem of transforming $\hat{A}(k)$ under $\hat{B}_N$ is reduced to the (kth) one-electron vector space and, according to Eqs. (A4, A18), can be stated in the form

$$\hat{B}^{\dagger}\hat{A}\hat{B}=(\hat{L}_{\bigcirc}-\hat{L}_{*})\hat{A}(\hat{L}_{\bigcirc}-\hat{L}_{*})=\hat{A}_{+}-\hat{A}_{-}. \quad \text{(A21)}$$

The operator $\hat{K}'$, obtained from $\hat{K}$ by changing all creation operators to annihilation operators and vice versa, obeys the property [68]

$$\hat{K}\hat{D}-\hat{D}\hat{K}'=\hat{0}. \quad \text{(A22)}$$

Multiplication by $\hat{D}^{\dagger}$ yields

$$\hat{K}'=\hat{D}^{\dagger}\hat{K}\hat{D}. \quad \text{(A23)}$$

If $\hat{K}$ is a one-electron Hermitian operator

$$\hat{K}=\sum_{i,j}\langle i|\hat{K}|j\rangle a_i^{\dagger}a_j \quad \text{(A24)}$$

with real matrix elements $\langle i|\hat{K}|j\rangle$, it holds (according to the fermion creation and annihilation anticommutation rules)

$$\hat{K}' = \mathrm{Tr}(\hat{K})\hat{I} - \hat{K}, \quad \mathrm{Tr}(\hat{K}) = \sum_i \langle i|\hat{K}|i\rangle. \tag{A25}$$

The transformation rules (A25) hold for operators $\hat{A}_+$ and $\hat{A}_-$ as defined by Eq. (A19) and, therefore, any one-electron Hermitian operator $\hat{A}$ is transformed under alternancy conjugation according to

$$\hat{P}^\dagger \hat{A} \hat{P} = \hat{D}^\dagger (A_+ - A_-)\hat{D} = \mathrm{Tr}(\hat{A}_+)\hat{I} - Tr(\hat{A}_-)\hat{I} - \hat{A}_+ + \hat{A}_-. \tag{A26}$$

From Eq. (A15) follows then

$$\langle x|\hat{A}|y\rangle = \pm[\mathrm{Tr}(\hat{A}_+) - \mathrm{Tr}(\hat{A}_-)]\langle x|y\rangle \mp \langle x|\hat{A}_+|y\rangle \pm \langle x|\hat{A}_-|y\rangle. \tag{A27}$$

4. Selection rules

We consider now how the carotenoid matrix elements ${}^kM(i,i)$ and ${}^kM(i,j)$, defined in Eqs. (2.19,2.20), transform under alternancy conjugation. It is convenient to consider, instead of ${}^kM(i,j), i \neq j$ the elements ${}^kM(i,j) + {}^kM(j,i)$, which correspond to the tensor operators ${}^{km}\hat{O}_{ij} + {}^{km}\hat{O}_{ji} = {}^{km}\hat{O}'_{ij}$ in Eqs. (2.19,2.20).

The two tensor operators involving atomic orbitals i and j can be written

$${}^{11}\hat{O}'_{ij} = -|i\rangle|\alpha\rangle\langle j|\langle\beta| - |j\rangle|\beta\rangle\langle i|\langle\alpha|, \tag{A28}$$

$${}^{00}\hat{O}'_{ij} = \sum_{\eta=\alpha,\beta} (|i\rangle|\eta\rangle\langle j|\langle\eta| + |j\rangle|\eta\rangle\langle i|\langle\eta|). \tag{A29}$$

Choosing the eigenstates orthogonal, i.e., $\langle x|y\rangle = \delta_{xy}$, and inserting $\hat{O}'_{ij}$ into expression (A26)

$$\langle x|\hat{O}'_{ij}|y\rangle = \mp\langle x|(\hat{O}_+)'_{ij}|y\rangle \pm \langle x|(\hat{O}_-)'_{ij}|y\rangle. \tag{A30}$$

The upper sign applies in the case of an $2^1A_g^- \rightarrow 1^1A_g^-$ transition since the states $1^1A_g^-$ and $2^1A_g^-$ have the same alternancy symmetry; the lower sign applies to transitions $1^1B_u^+ \rightarrow 1^1A_g^-$ and $1^1A_g^- \rightarrow 1^3B_u^+$ since the respective states have different alternancy symmetry. We have omitted the spin indices since Eq. (A30) is independent of spin.

Two cases can be distinguished for the combinations of atomic orbital indices i and j. In the first case, i and j belong to the same set of atomic orbitals (starred or unstarred). In this case holds, due to the orthogonality of atomic orbitals,

$$(\hat{O}_-)'_{ij} = \hat{L}_\bigcirc \hat{O}'_{ij} \hat{L}_* + \hat{L}_* \hat{O}'_{ij} \hat{L}_\bigcirc = 0. \tag{A31}$$

From Eq. (A18) it follows that

$$\hat{O}'_{ij} = (\hat{O}_+)'_{ij}, \tag{A32}$$

and Eq. (A30) imposes the selection rules

$$\langle x|\hat{O}'_{ij}|y\rangle = \mp\langle x|\hat{O}'_{ij}|y\rangle. \tag{A33}$$

Accordingly, the matrix elements ${}^kM(i,j) + {}^kM(j,i)$ in Eq. (2.19,2.20) for i,j belonging to the same set of either starred or unstarred atoms, vanish in case of the $2^1A_g^- \rightarrow 1^1A_g^-$ transition.

In the second case, i and j belong to the opposite sets, i.e., i labels a ''starred'' atom and j an ''unstarred'' atom or vice versa. In this case the operator $\hat{O}_{ij}$ obeys

$$(\hat{O}_+)'_{ij} = \hat{L}_\bigcirc \hat{O}'_{ij} \hat{L}_\bigcirc + \hat{L}_* \hat{O}'_{ij} \hat{L}_* = 0 \tag{A34}$$

and from Eq. (A18) it follows that

$$\hat{O}'_{ij} = (\hat{O}_-)'_{ij}. \tag{A35}$$

This leads to the condition

$$\langle x|\hat{O}'_{ij}|y\rangle = \pm\langle x|\hat{O}'_{ij}|y\rangle. \tag{A36}$$

Accordingly, the matrix elements ${}^kM(i,j) + {}^kM(j,i)$ in Eqs. (2.19,2.20) for i,j connecting a starred and an unstarred atom, vanish in case of the transitions $1^1B_u^+ \rightarrow 1^1A_g^-$ and $1^1A_g^- \rightarrow 1^3B_u^+$.

[1] X. Hu and K. Schulten, Phys. Today **50** (8), 28 (1997).
[2] X. Hu, A. Damjanović, T. Ritz, and K. Schulten, Proc. Natl. Acad. Sci. USA **95**, 5935 (1998).
[3] E. Hofmann *et al.*, Science **272**, 1788 (1996).
[4] M. Griffiths, W. Sistrom, G. Cohen-Bazire, and R. Y. Stanier, Nature (London) **176**, 1211 (1955).
[5] W. R. Sistrom, M. Griffiths, and R. Y. Stanier, J. Cell. Comp. Physiol. **48**, 473 (1956).
[6] N. I. Krinsky, Pure Appl. Chem. **51**, 649 (1979).
[7] R. J. Cogdell and H. A. Frank, Biochim. Biophys. Acta **895**, 63 (1987).
[8] N. A. Krinsky, in *The Survival of Vegetative Microbes*, edited by T. G. R. Gray and J. R. Postgate (Cambridge Univ. Press, Cambridge, 1976), pp. 209–239.
[9] G. McDermott *et al.*, Nature (London) **374**, 517 (1995).
[10] J. Koepke *et al.*, Structure **4**, 581 (1996).
[11] A. P. Shreve *et al.*, Biochim. Biophys. Acta **1058**, 280 (1991).
[12] X. Hu, T. Ritz, A. Damjanović, and K. Schulten, J. Phys. Chem. B **101**, 3854 (1997).
[13] M. Kuki, H. Nagae, R. Cogdell, and Y. Koyama, Photochem. Photobiol. **59**, 116 (1994).
[14] P. Tavan and K. Schulten, J. Chem. Phys. **85**, 6602 (1986).
[15] B. S. Hudson, B. E. Kohler, and K. Schulten, in *Excited States*, edited by E. C. Lim (Academic Press, New York, 1982), Vol. 6, pp. 1–95.
[16] P. Tavan and K. Schulten, J. Chem. Phys. **70**, 5407 (1979).
[17] P. Tavan and K. Schulten, Phys. Rev. B **36**, 4337 (1987).
[18] P. Tavan and K. Schulten, in *Nonlinear Optical Properties of Polymers*, MRS Symposium Proceedings No. 109, edited by A. J. Heeger, J. Orenstein, and D. Ulrich (Materials Research Society, Pittsburgh, 1988), pp. 163–170.
[19] T. Gillbro *et al.*, Photochem. Photobiol. **57**, 44 (1993).

[20] Y. Koyama, M. Kuki, P. Andersson, and T. Gillbro, Photochem. Photobiol. **63**, 243 (1996).
[21] B. W. Chadwick, C. Zhang, R. J. Cogdell, and H. A. Frank, Biochim. Biophys. Acta **893**, 444 (1987).
[22] A. P. Shreve, J. K. Trautman, T. G. Owens, and A. C. Albrecht, Chem. Phys. Lett. **178**, 89 (1991).
[23] M. Ricci, S. E. Bradforth, R. Jimenez, and G. R. Fleming, Chem. Phys. Lett. **259**, 381 (1996).
[24] T. Sashima, H. Nagae, M. Kuki, and Y. Koyama (unpublished).
[25] T. Förster, Ann. Phys. (Leipzig) **2**, 55 (1948).
[26] B. P. Krueger, G. D. Scholes, and G. R. Fleming, J. Phys. Chem. B **102**, 5378 (1998).
[27] H. Nagae, T. Kakitani, T. Katohi, and M. Mimuro, J. Chem. Phys. **98**, 8012 (1993).
[28] D.L. Dexter, J. Chem. Phys. **21**, 836 (1963)
[29] R. van Grondelle, J. Dekker, T. Gillbro, and V. Sundstrom, Biochim. Biophys. Acta **1187**, 1 (1994).
[30] K. R. Naqvi, Photochem. Photobiol. **31**, 523 (1980).
[31] C. S. Foote, Y. C. Chang, and R. W. Denny, J. Am. Chem. Soc. **92**, 5216 (1970).
[32] C. S. Foote, Free Radicals Biol. **2**, 85 (1976).
[33] M. Chessin, R. Livingston, and T. G. Truscott, Trans. Faraday Soc. **62**, 1519 (1966).
[34] H. T. Witt, Q. Rev. Biophys. **4**, 365 (1971).
[35] R. Bensasson, E. J. Land, and B. Maudinas, Photochem. Photobiol. **23**, 189 (1976).
[36] P. Mathis and J. Kleo, Photochem. Photobiol. **18**, 343 (1973).
[37] H. Claes and T. O. M. Nakayama, Z. Naturforsch. B **14**, 746 (1959).
[38] H. Claes, Biochem. Biophys. Res. Commun. **3**, 585 (1960).
[39] M. M. Mathews-Roth and N. I. Krinsky, Photochem. Photobiol. **11**, 419 (1970).
[40] T. G. Monger, R. J. Cogdell, and W. W. Parson, Biochim. Biophys. Acta **449**, 136 (1976).
[41] K. Schulten, I. Ohmine, and M. Karplus, J. Chem. Phys. **64**, 4422 (1976).
[42] K. Schulten and M. Karplus, Chem. Phys. Lett. **14**, 305 (1972).
[43] W. Weber, Ph.D. thesis, Universität Zürich, Philosphische Fakultät II, Zürich, Switzerland, 1996.
[44] G. D. Scholes, K. P. Ghiggino, A. M. Oliver, and M. N. Padden-Row, J. Phys. Chem. **87**, 11 871 (1993).
[45] S. Larsson, J. Am. Chem. Soc. **103**, 4034 (1981).
[46] Author(s), in *QUANTA 97* (Molecular Simulations Inc., Burlington, Massachusetts, 1997).
[47] J. Jortner, S. A. Rice, and J. L. Katz, J. Chem. Phys. **42**, 309 (1965).
[48] A. Szabo and N. Ostlund, *Modern Quantum Chemistry: Introduction to Advanced Electronic Structure Theory* (MacMillan, New York, 1982).
[49] *CERN Program Library Long Writeup Y250*, CERN, 1994.
[50] J. O. Hirschfelder and J. W. Linnett, J. Chem. Phys. **18**, 130 (1949).
[51] M. C. Zerner, M. G. Cory, X. Hu, and K. Schulten, J. Phys. Chem. B **102**, 7640 (1998).
[52] H. Wu and G. Small, J. Phys. Chem. **102**, 888 (1998).
[53] L. Germeroth, F. Lottspeich, B. Robert, and H. Michel, Biochemistry **32**, 5615 (1993).
[54] H. Frank *et al.*, Pure Appl. Chem. **68**, 2117 (1997).
[55] M. Mimuro *et al.*, Biochim. Biophys. Acta **1098**, 271 (1992).
[56] C. D. Caro, R. W. Visschers, R. van Grondelle, and S. Völker, J. Phys. Chem. **98**, 10 584 (1994).
[57] P. O. Anderson, T. Gillbro, L. Ferguson, and R. J. Cogdell, Photochem. Photobiol. **54**, 353 (1991).
[58] K. Sauer, J. R. L. Smith, and A. J. Schultz, J. Am. Chem. Soc. **88**, 2681 (1966).
[59] R. J. Cogdell, P. O. Andersson, and T. Gillbro, J. Photochem. Photobiol., B **15**, 105 (1992).
[60] H. Frank and R. Cogdell, Photochem. Photobiol. **63**, 257 (1996).
[61] Z. Zhang *et al.*, Nature (London) **392**, 677 (1998).
[62] R. Jimenez, S. Dikshit, S. Bradforth, and G. Fleming, J. Phys. Chem. **100**, 6825 (1996).
[63] D. Leupold *et al.*, Phys. Rev. Lett. **77**, 4675 (1996).
[64] P. D. Laible *et al.*, Biophys. J. **74**, 2623 (1998).
[65] W. Kuhlbrandt, in *Membrane Protein Structure: Experimental Approaches*, edited by S. White (Oxford University Press, New York, 1994), pp. 206–223.
[66] J. B. Arellano, R. B. Raju, K. R. Naqvi, and T. Gillbro, Photochem. Photobiol. **68**, 84 (1998).
[67] J. Cizek, J. Paldus, and I. Hubac, Int. J. Quantum Chem. **8**, 951 (1974).
[68] J. Koutecky, J. Chem. Phys. **44**, 3702 (1996).
[69] R. Pariser, J. Chem. Phys. **24**, 250 (1956).
[70] W. F. Humphrey, A. Dalke, and K. Schulten, J. Mol. Graphics **14**, 33 (1996).